

# Fundamental limits on the rate of bacterial cell division

<sup>3</sup> **Nathan M. Belliveau<sup>†, 1</sup>, Griffin Chure<sup>†, 2, 3</sup>, Christina L. Hueschen<sup>4</sup>, Hernan G.  
<sup>4</sup> Garcia<sup>5</sup>, Jané Kondev<sup>6</sup>, Daniel S. Fisher<sup>7</sup>, Julie Theriot<sup>1, 8</sup>, Rob Phillips<sup>2, 9, \*</sup>**

\*For correspondence:

<sup>†</sup>These authors contributed equally to this work

<sup>5</sup> <sup>1</sup>Department of Biology, University of Washington, Seattle, WA, USA; <sup>2</sup>Division of  
<sup>6</sup> Biology and Biological Engineering, California Institute of Technology, Pasadena, CA,  
<sup>7</sup> USA; <sup>3</sup>Department of Applied Physics, California Institute of Technology, Pasadena, CA,  
<sup>8</sup> USA; <sup>4</sup>Department of Chemical Engineering, Stanford University, Stanford, CA, USA;  
<sup>9</sup> <sup>5</sup>Department of Molecular Cell Biology and Department of Physics, University of  
<sup>10</sup> California Berkeley, Berkeley, CA, USA; <sup>6</sup>Department of Physics, Brandeis University,  
<sup>11</sup> Waltham, MA, USA; <sup>7</sup>Department of Applied Physics, Stanford University, Stanford, CA,  
<sup>12</sup> USA; <sup>8</sup>Allen Institute for Cell Science, Seattle, WA, USA; <sup>9</sup>Department of Physics,  
<sup>13</sup> California Institute of Technology, Pasadena, CA, USA; \*Contributed equally

<sup>14</sup> 

---

<sup>15</sup> **Abstract** This will be written next

<sup>16</sup> 

---

## <sup>17</sup> Introduction

<sup>18</sup> The range of bacterial growth rates is enormously diverse. In natural environments, some micro-  
<sup>19</sup> bial organisms might double only once per year while in comfortable laboratory conditions, growth  
<sup>20</sup> can be rapid with several divisions per hour. This six order of magnitude difference illustrates the  
<sup>21</sup> intimate relationship between environmental conditions and the rates at which cells convert nutri-  
<sup>22</sup> ents into new cellular material – a relationship that has remained a major topic of inquiry in bac-  
<sup>23</sup> terial physiology for over a century (?). As was noted by Jacques Monod, “the study of the growth  
<sup>24</sup> of bacterial cultures does not constitute a specialized subject or branch of research, it is the ba-  
<sup>25</sup> sic method of Microbiology.” Those words ring as true today as they did when they were written  
<sup>26</sup> 70 years ago. Indeed, the study of bacterial growth has undergone a molecular resurgence since  
<sup>27</sup> many of the key questions addressed by the pioneering efforts in the middle of the last century  
<sup>28</sup> can be revisited by examining them through the lens of the increasingly refined molecular census  
<sup>29</sup> that is available for bacteria such as the microbial workhorse *Escherichia coli*. Several of the out-  
<sup>30</sup> standing questions that can now be studied about bacterial growth include: what sets the fastest  
<sup>31</sup> time scale that bacteria can divide, and how is growth rate tied to the quality of the carbon source.  
<sup>32</sup> In this paper, we address these two questions from two distinct angles. First, as a result of an array  
<sup>33</sup> of high-quality proteome-wide measurements of the *E. coli* proteome under a myriad of different  
<sup>34</sup> growth conditions, we have a census that allows us to explore how the number of key molecular  
<sup>35</sup> players change as a function of growth rate. This census provides a window onto whether the  
<sup>36</sup> processes they mediate such as molecular transport into the cells and molecular synthesis within  
<sup>37</sup> cells can run faster. Second, because of our understanding of the molecular pathways responsi-  
<sup>38</sup> ble for many of the steps in bacterial growth, we can also make order of magnitude estimates to  
<sup>39</sup> infer the copy numbers that would be needed to achieve a given growth rate. In this paper, we  
<sup>40</sup> pass back and forth between the analysis of a variety of different proteomic datasets and order-  
<sup>41</sup> of-magnitude estimations to determine possible molecular bottlenecks that limit bacterial growth

42 and to see how the growth rate varies in different carbon sources.

43 Specifically, we leverage a combination of *E. coli* proteomic data sets collected over the past  
 44 decade using either mass spectrometry (???) or ribosomal profiling (?) across 31 unique growth  
 45 conditions. Broadly speaking, we entertain several classes of hypotheses as are illustrated in **Figure 1**.  
 46 First, we consider potential limits on the transport of nutrients into the cell. We address this  
 47 hypothesis by performing an order-of-magnitude estimate for how many carbon, phosphorous,  
 48 and sulfur atoms are needed to facilitate this requirement given a 5000 second division time. As a  
 49 second hypothesis, we consider the possibility that there exists a fundamental limit on how quickly  
 50 the cell can generate ATP. We approach this hypothesis from two angles, considering how many  
 51 ATP synthase complexes must be needed to churn out enough ATP to power protein translation  
 52 followed by an estimation of how many electron transport complexes must be present to main-  
 53 tain the proton motive force. A third class of estimates considers the need to maintain the size  
 54 and shape of the cell through the construction of new lipids for the cell membranes as well as the  
 55 glycan polymers which make up the rigid peptidoglycan. Our final class of hypotheses centers on  
 56 the synthesis of a variety of biomolecules. Our focus is primarily on the stages of the central dogma  
 57 as we estimate the number of protein complexes needed for DNA replication, transcription, and  
 58 protein translation.

59 In broad terms, we find that the majority of these estimates are in close agreement with the  
 60 experimental observations, with protein copy numbers apparently well-tuned for the task of cell  
 61 doubling. This allows us to systematically scratch off the hypotheses diagrammed in **Figure 1** as  
 62 setting possible speed limits. Ultimately, we find that protein translation (particularly the genera-  
 63 tion of new ribosomes) acts as 1) a rate limiting step for the *fastest* bacterial division, and 2) the  
 64 major determinant of bacterial growth across all nutrient conditions we have considered under  
 65 steady state, exponential growth. This perspective is in line with the linear correlation observed  
 66 between growth rate and ribosomal content (typically quantified through the ratio of RNA to pro-  
 67 tein) for fast growing cells (?), but suggests a more prominent role for ribosomes in setting the  
 68 doubling time across all conditions of nutrient limitation. Here we again leverage the quantitative  
 69 nature of this data set and present a quantitative model of the relationship between the fraction  
 70 of the proteome devoted to ribosomes and the speed limit of translation, revealing a fundamental  
 71 tradeoff between the translation capacity of the ribosome pool and the maximal growth rate.

## 72 Uptake of Nutrients

73 In order to build new cellular mass, the molecular and elemental building blocks must be scav-  
 74 enged from the environment in different forms. Carbon, for example, is acquired via the transport  
 75 of carbohydrates and sugar alcohols with some carbon sources receiving preferential treatment  
 76 in their consumption (?). Phosphorus, sulfur, and nitrogen, on the other hand, are harvested pri-  
 77 marily in the forms of inorganic salts, namely phosphate, sulfate, and ammonia (??????). All of  
 78 these compounds have different permeabilities across the cell membrane and most require some  
 79 energetic investment either via ATP hydrolysis or through the proton electrochemical gradient to  
 80 bring the material across the hydrophobic cell membrane. Given the diversity of biological trans-  
 81 port mechanisms and the vast number of inputs needed to build a cell, we begin by considering  
 82 transport of some of the most important cellular ingredients: carbon, nitrogen, oxygen, hydrogen,  
 83 phosphorus, and sulfur.

84 The elemental composition of *E. coli* has received much quantitative attention over the past  
 85 half century (????), providing us with a starting point for estimating the copy numbers of various  
 86 transporters. While there is some variability in the exact elemental percentages (with different un-  
 87 certainties), we can estimate that the dry mass of a typical *E. coli* cell is  $\approx$  45% carbon (BNID: 100649,  
 88 ?),  $\approx$  15% nitrogen (BNID: 106666, ?),  $\approx$  3% phosphorus (BNID: 100653, ?), and 1% sulfur (BNID:  
 89 100655, ?). In the coming paragraphs, we will engage in a dialogue between back-of-the-envelope  
 90 estimates for the numbers of transporters needed to facilitate these chemical stoichiometries and  
 91 the experimental proteomic measurements of the biological reality. Such an approach provides

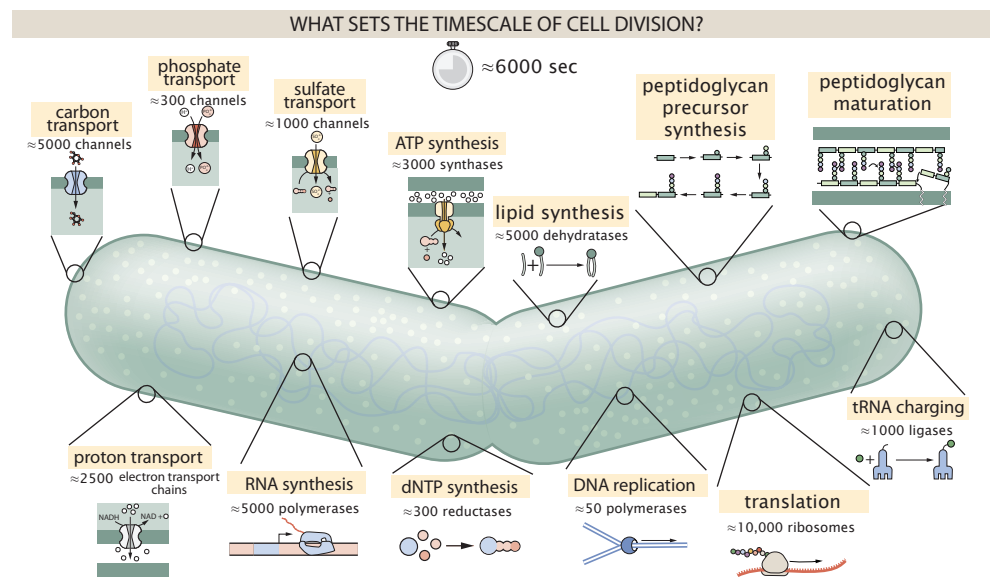


**Figure 1. Transport and synthesis processes necessary for cell division.** We consider an array of processes necessary for a cell to double its molecular components. Such processes include the transport of carbon across the cell membrane, the production of ATP, and fundamental processes of the central dogma namely RNA, DNA, and protein synthesis. A schematic of each synthetic or transport category is shown with an approximate measure of the complex abundance at a growth rate of 0.5 per hour. In this work, we consider a standard bacterial division time of  $\approx 5000$  sec.

the opportunity to test if our biological knowledge is sufficient to understand the scale at which these complexes are produced. Specifically, we will make these estimates considering a modest doubling time of 5000 s, a growth rate of  $\approx 0.5 \text{ hr}^{-1}$ , the range in which the majority of the experimental measurements reside.

### Nitrogen Transport

Before we begin our back-of-the-envelope estimations, we must address which elemental sources must require proteinaceous transport, meaning that the cell cannot acquire appreciable amounts simply via diffusion from the membrane. The permeability of the lipid membrane to a large number of solutes has been extensively characterized over the past century. Large, polar molecular species (such as various sugar molecules, sulfate, and phosphate) have low permeabilities while small, non-polar compounds (such as oxygen, carbon dioxide, and ammonia) can readily diffuse across the membrane. Ammonia, a primary source of nitrogen in typical laboratory conditions, has a permeability on par with water ( $\approx 10^5 \text{ nm/s}$ , BNID:110824 ?). In particularly nitrogen-poor conditions, *E. coli* expresses a transporter (AmtB) which appears to aid in nitrogen assimilation, though the mechanism and kinetic details of transport is still a matter of debate (??). Beyond ammonia, another plentiful source of nitrogen come in the form of glutamate, which has its own complex metabolism and scavenging pathways. However, nitrogen is plentiful in the growth conditions examined in this work, permitting us to neglect nitrogen transport as a potential rate limiting process in cell division in typical experimental conditions. We direct the reader to the supplemental information for a more in-depth discussion of permeabilities and a series of calculations revealing that active nitrogen transport can be neglected for the purposes of this article.

### Carbon Transport

We begin our estimations with the most abundant element in *E. coli* by mass, carbon. Using  $\approx 0.3 \text{ pg}$  as the typical *E. coli* dry mass (BNID: 103904, ?), we estimate that  $\approx 10^{10}$  carbon atoms must be brought into the cell in order to double all of the carbon-containing molecules (Figure 2(A, top))). Typical laboratory growth conditions, such as those explored in the aforementioned proteomic

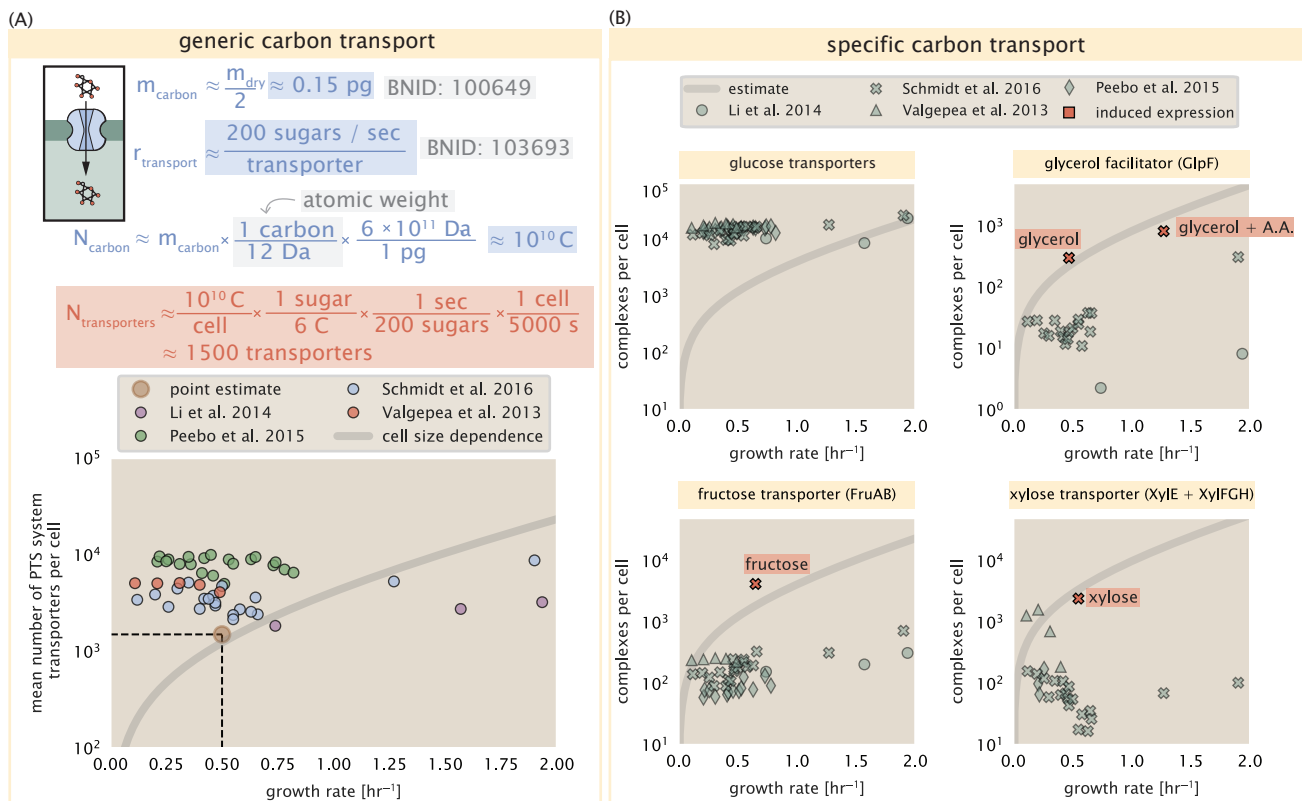


**Figure 2. The abundance of carbon transport systems across growth rates.** (A) A simple estimate for the minimum number of generic carbohydrate transport systems (top) assumes  $\approx 10^{10}$  C are needed to complete division, each transported sugar contains  $\approx 6$  C, and each transporter conducts sugar molecules at a rate of  $\approx 200$  per second. Bottom plot shows the estimated number of transporters needed at a growth rate of  $\approx 0.5$  per hr (light-brown point and dashed lines). Colored points correspond to the mean number of PTS system sugar transporters (complexes annotated with the Gene Ontology term GO:0009401) for different growth conditions across different published datasets. (B) The abundance of various specific carbon transport systems plotted as a function of the population growth rate. Red points and red-highlighted text indicate conditions in which the only source of carbon in the growth medium induces expression of the transport system. Grey line in (A) and (B) represents the estimated number of transporters per cell at a continuum of growth rates.

118 data sets, provide carbon as a single class of sugar such as glucose, galactose, or xylose to name a  
 119 few. *E. coli* has evolved myriad mechanisms by which these sugars can be transported across the  
 120 cell membrane. One such mechanism of transport is via the PTS system which is a highly modu-  
 121 lar system capable of transporting a diverse range of sugars (?). The glucose-specific component  
 122 of this system transports  $\approx 200$  glucose molecules per second per transporter (BNID: 114686, ?).  
 123 Making the assumption that this is a typical sugar transport rate, coupled with the need to trans-  
 124 port  $10^{10}$  carbon atoms, we arrive at the conclusion that on the order of 1,000 transporters must  
 125 be expressed in order to bring in enough carbon atoms to divide in 5000 s, diagrammed in the  
 126 top panel of **Figure 2(A)**. This estimate, along with the observed average number of the PTS sys-  
 127 tem carbohydrate transporters present in the proteomic data sets (????), is shown in **Figure 2(A)**.  
 128 While we estimate 1500 transporters are needed with a 5000 s division time, we can abstract this  
 129 calculation to consider any particular growth rate given knowledge of the cell density and volume  
 130 as a function of growth rate and direct the reader to the SI for more information. As revealed  
 131 in **Figure 2(A)**, experimental measurements exceed the estimate by several fold, illustrating that  
 132 transport of carbon in to the cell is not rate limiting for cell division.

133 The estimate presented in **Figure 2(A)** neglects any specifics of the regulation of carbon trans-

port system and presents a data-averaged view of how many carbohydrate transporters are present on average. Using the diverse array of growth conditions explored in the proteomic data sets, we can explore how individual carbon transport systems depend on the population growth rate. In **Figure 2(B)**, we show the total number of carbohydrate transporters specific to different carbon sources. A striking observation, shown in the top-left plot of **Figure 2(B)**, is the constancy in the expression of the glucose-specific transport systems. Additionally, we note that the total number of glucose-specific transporters is tightly distributed  $\approx 10^4$  per cell, the approximate number of transporters needed to sustain rapid growth of several divisions per hour, as indicated by the grey shaded line. This illustrates that *E. coli* maintains a substantial number of complexes present for transporting glucose which is known to be the preferential carbon source (??).

It is now understood that a large number of metabolic operons are regulated with dual-input logic gates that are only expressed when glucose concentrations are low (mediated by cyclic-AMP receptor protein CRP) and the concentration of other carbon sources are elevated (??). A famed example of such dual-input regulatory logic is in the regulation of the *lac* operon which is only natively activated in the absence of glucose and the presence of allolactose, an intermediate in lactose metabolism (?), though we now know of many other such examples (??). This illustrates that once glucose is depleted from the environment, cells have a means to dramatically increase the abundance of the specific transporter needed to digest the next sugar that is present. Several examples of induced expression of specific carbon-source transporters are shown in **Figure 2(B)**. Points colored in red (labeled by red text-boxes) correspond to growth conditions in which the specific carbon source (glycerol, xylose, or fructose) is present. These plots show that, in the absence of the particular carbon source, expression of the transporters is maintained on the order of  $\sim 10^2$  per cell. However, when induced, the transporters become highly-expressed and fall close to the predicted number of transporters needed to facilitate growth on that substrate alone, shown as a transparent grey line. Together, this generic estimation and the specific examples of induced expression suggest that transport of carbon across the cell membrane, while critical for growth, is not the rate-limiting step of cell division.

### 161 Phosphorus and Sulfur Transport

162 We now turn our attention towards other essential elements, namely phosphorus and sulfur. Phosphorus is critical to the cellular energy economy in the form of high-energy phosphodiester bonds 163 making up DNA, RNA, and the NTP energy pool as well as playing a critical role in the post-translational 164 modification of proteins and defining the polar-heads of lipids. In total, phosphorus makes up 165  $\approx 3\%$  of the cellular dry mass which in typical experimental conditions is in the form of inorganic 166 phosphate. The cell membrane has remarkably low permeability to this highly-charged and critical 167 molecule, therefore requiring the expression of active transport systems. In *E. coli*, the proton elec- 168 trochemical gradient across the inner membrane is leveraged to transport inorganic phosphate 169 into the cell (?). Proton-solute symporters are widespread in *E. coli* (??) and can have rapid trans- 170 port rates of 50 to 100 molecules per second for sugars and other solutes (BNID: 103159; 111777, ?). 171 As a more extreme example, the proton transporters in the F<sub>1</sub>-F<sub>0</sub> ATP synthase, which leverage the 172 proton electrochemical gradient for rotational motion, can shuttle protons across the membrane 173 at a rate of  $\approx 1000$  per second (BNID: 104890; 103390, (?)). In *E. coli* the PitA phosphate transport 174 system has been shown to be very tightly coupled with the proton electrochemical gradient with a 175 1:1 proton:phosphate stoichiometric ratio (??). Taking the geometric mean of the aforementioned 176 estimates gives a plausible rate of phosphate transport on the order of 300 per second. Illustrated 177 in **Figure 3(A)**, we can estimate that  $\approx 150$  phosphate transporters are necessary to maintain an 178  $\approx 3\%$  dry mass with a 5000 s division time. This estimate is again satisfied when we examine the 179 observed copy numbers of PitA in proteomic data sets (plot in **Figure 3(A)**). While our estimate is 180 very much in line with the observed numbers, we emphasize that this is likely a slight overestimate 181 of the number of transporters needed as there are other phosphorous scavenging systems, such 182 as the ATP-dependent phosphate transporter Pst system which we have neglected.

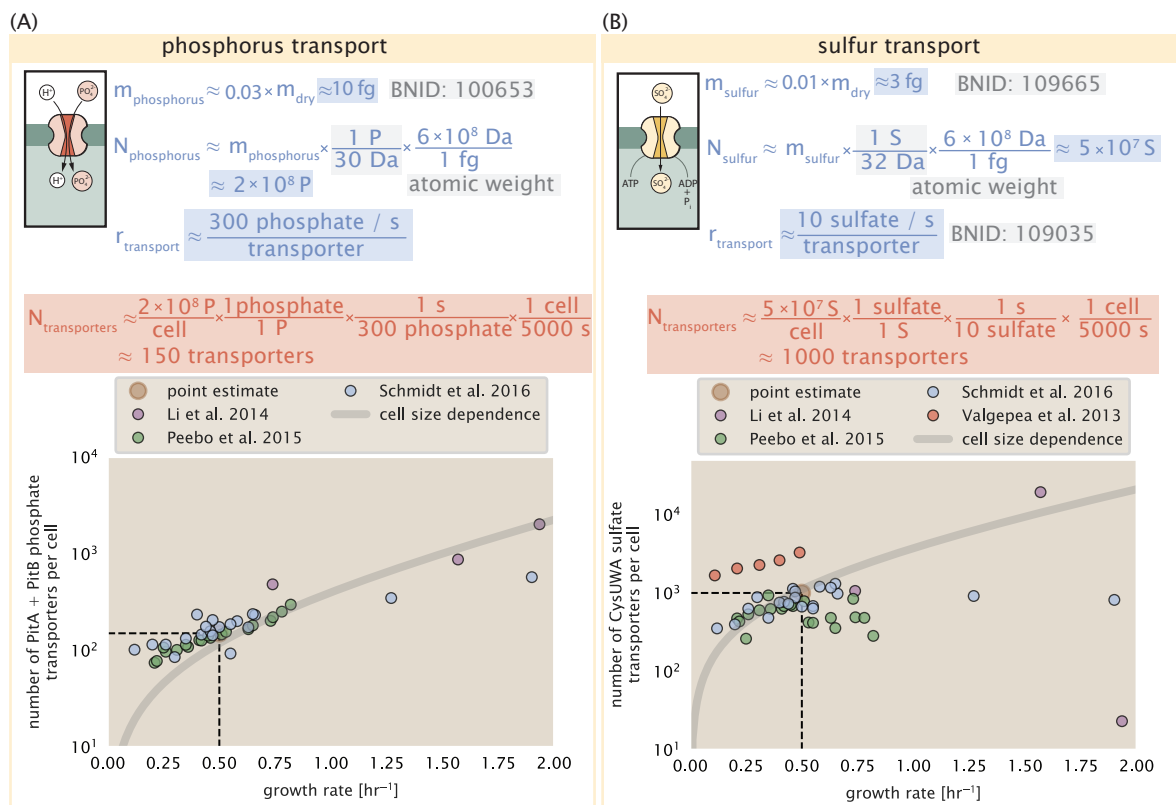


**Figure 3. Estimates and measurements of phosphate and sulfate transport systems as a function of growth rate.** (A) Estimate for the number of PitA phosphate transport systems needed to maintain a 3% phosphorus *E. coli* dry mass. Points in plot correspond to the total number of PitA transporters per cell. (B) Estimate of the number of CysUWA complexes necessary to maintain a 1% sulfur *E. coli* dry mass. Points in plot correspond to average number of CysUWA transporter complexes that can be formed given the transporter stoichiometry [CysA]<sub>2</sub>[CysU][CysW][Sbp/CysP]. Grey line in (A) and (B) represents the estimated number of transporters per cell at a continuum of growth rates.

184 Satisfied that there are a sufficient number of phosphate transporters present in the cell, we  
 185 now turn to sulfur transport as another potentially rate limiting process. Similar to phosphate, sul-  
 186 fide is highly-charged and not particularly membrane permeable, requiring active transport. While  
 187 there exists a H<sup>+</sup>/sulfate symporter in *E. coli*, it is in relatively low abundance and is not well char-  
 188 acterized (?). Sulfate is predominantly acquired via the ATP-dependent ABC transporter CysUWA  
 189 system which also plays an important role in selenium transport (??). While specific kinetic details  
 190 of this transport system are not readily available, generic ATP transport systems in prokaryotes  
 191 transport on the order of 1 to 10 molecules per second (BNID: 109035, ?). Combining this generic  
 192 transport rate, measurement of sulfur comprising 1% of dry mass, and a 5000 second division time  
 193 yields an estimate of  $\approx 1000$  CysUWA complexes per cell (Figure 3(B)). Once again, this estimate is  
 194 in notable agreement with proteomic data sets, suggesting that there are sufficient transporters  
 195 present to acquire the necessary sulfur. In a similar spirit of our estimate of phosphorus transport,  
 196 we emphasize that this is likely an overestimate of the number of necessary transporters as we  
 197 have neglected other sulfur scavenging systems that are in lower abundance.

#### 198 **Limits on Transporter Expression**

199 So which, if any, of these processes may be rate limiting for growth? As suggested by Figure 2  
 200 (B), induced expression can lead to an order-of-magnitude (or more) increase in the amount of  
 201 transporters needed to facilitate transport. Thus, if acquisition of nutrients was the limiting state  
 202 in cell division, could expression simply be increased to accommodate faster growth? A way to

203 approach this question is to compute the amount of space in the bacterial membrane that could  
 204 be occupied by nutrient transporters. Considering a rule-of-thumb for the surface area of *E. coli* of  
 205 about  $6 \mu\text{m}^2$  (BNID: 101792, ?), we expect an areal density for 1000 transporters to be approximately  
 206 200 transporters/ $\mu\text{m}^2$ . For a typical transporter occupying about  $50 \text{ nm}^2/\text{dimer}$ , this amounts to  
 207 about only 1 percent of the total inner membrane (?). In addition, bacterial cell membranes typically  
 208 have densities of  $10^5 \text{ proteins}/\mu\text{m}^2$  (?), implying that the cell could accommodate more transporters  
 209 of a variety of species if it were rate limiting. As we will see in the next section, however, occupancy  
 210 of the membrane can impose other limits on the rate of energy production.

## 211 Energy Production

212 While the transport of nutrients is required to build new cell mass, the metabolic pathways involved in assimilation both consumes and generates energy in the form of NTPs. The high-energy  
 213 phosphodiester bonds of (primarily) ATP power a variety of cellular processes that drive biological  
 214 systems away from thermodynamic equilibrium. Our next class of estimates consider the energy  
 215 budget of a dividing cell in terms of the synthesis of ATP from ADP and inorganic phosphate as well  
 216 as maintenance of the electrochemical proton gradient which powers it.

## 218 ATP Synthesis

219 Hydrolysis of the terminal phosphodiester bond of ATP forming ADP and an inorganic phosphate is  
 220 a kinetic driving force in a wide array of biochemical reactions. One such reaction is the formation  
 221 of peptide bonds during translation which requires  $\approx 2$  ATPs for the charging of an amino acid  
 222 to the tRNA and  $\approx 2$  ATP equivalents for the formation of the peptide bond between amino acids.  
 223 Together, these energetic costs consume  $\approx 80\%$  of the cells ATP budget (BNID: 107782; 106158;  
 224 101637; 111918, ?). The pool of ATP is produced by the  $F_1$ - $F_0$  ATP synthase – a membrane-bound  
 225 rotary motor which under ideal conditions can yield  $\approx 300$  ATP per second (BNID: 114701; ??).

226 To estimate the total number of ATP equivalents consumed during a cell cycle, we will make  
 227 the approximation that there are  $\approx 3 \times 10^6$  proteins per cell with an average protein length of  $\approx$   
 228 300 peptide bonds (BNID: 115702; 108986; 104877, ?). Taking these values together, we estimate  
 229 that the typical *E. coli* cell consumes  $\approx 5 \times 10^9$  ATP per cell cycle on protein synthesis alone and  
 230  $\approx 6 \times 10^9$  ATP in total. Assuming that the ATP synthases are operating at their fastest possible rate,  
 231  $\approx 3000$  ATP synthases are needed to keep up with the energy demands of the cell. This estimate  
 232 and a comparison with the data are shown in *Figure 4* (A). Despite our assumption of maximal ATP  
 233 production rate per synthase and approximation of all NTP consuming reactions being the same  
 234 as ATP, we find that an estimate of a few thousand complete synthases per cell to agree well with  
 235 the experimental data.

## 236 Generating the Proton Electrochemical Gradient

237 In order to produce ATP, the  $F_1$ - $F_0$  ATP synthase itself must consume energy. Rather than burning  
 238 through its own product, this intricate macromolecular machine has evolved to exploit the elec-  
 239 trochemical potential established across the inner membrane through cellular respiration. This  
 240 electrochemical gradient is manifest by the pumping of protons into the intermembrane space via  
 241 the electron transport chains as they reduce NADH. In *E. coli*, this potential difference is  $\approx -200$   
 242 mV (BNID: 102120, ?). As estimated in the supporting information, this potential difference is gen-  
 243 erated by maintaining  $\approx 2 \times 10^4$  protons in the intermembrane space.

244 However, the constant rotation of the ATP synthases would rapidly abolish this potential differ-  
 245 ence if it were not being actively maintained. To undergo a complete rotation (and produce a single  
 246 ATP), the  $F_1$ - $F_0$  ATP synthase must shuttle  $\approx 4$  protons across the membrane into the cytosol (BNID:  
 247 103390, ?). With  $\approx 3000$  ATP synthases each generating 300 ATP per second, the  $2 \times 10^4$  protons  
 248 establishing the 200 mV potential would be consumed in only a few milliseconds. This brings us to our  
 249 next estimate: how many electron transport complexes are needed to support the consumption  
 250 rate of the ATP synthases?

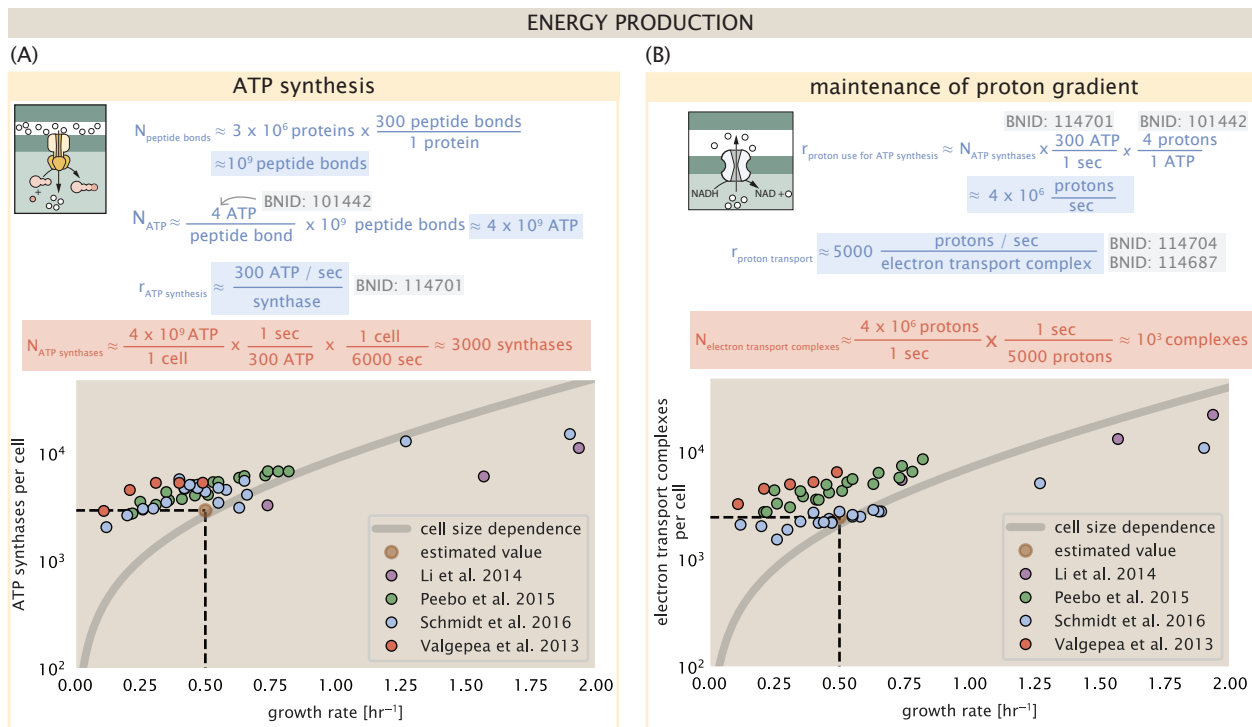


**Figure 4. The abundance of F<sub>1</sub>-F<sub>0</sub> ATP synthases and electron transport chain complexes as a function of growth rate.** (A) Estimate of the number of F<sub>1</sub>-F<sub>0</sub> ATP synthase complexes needed to accommodate peptide bond formation and other NTP dependent processes. Points in plot correspond to the mean number of complete F<sub>1</sub>-F<sub>0</sub> ATP synthase complexes that can be formed given proteomic measurements and the subunit stoichiometry [AtpE]<sub>10</sub>[AtpF]<sub>2</sub>[AtpB][AtpC][AtpH][AtpA]<sub>3</sub>[AtpG][AtpD]<sub>3</sub>. (B) Estimate of the number of electron transport chain complexes needed to maintain a membrane potential of  $-200$  mV given estimate of number of F<sub>1</sub>-F<sub>0</sub> ATP synthases from (A). Points in plot correspond to the average number of complexes identified as being involved in aerobic respiration by the Gene Ontology identifier GO:0019646 that could be formed given proteomic observations. These complexes include cytochromes bd1 ([CydA][CydB][CydX][CydH]), bdII ([AppC][AppB]), bo<sub>3</sub>,([CyoD][CyoA][CyoB][CyoC]) and NADH:quinone oxioreducase I ([NuoA][NuoH][NuoJ][NuoK][NuoL][NuoM][NuoN][NuoB][NuoC][NuoE][NuoF][NuoG][NuoI]) and II ([Ndh]).

251     The electrochemistry of the electron transport complexes of *E. coli* have been the subject of  
 252     intense biochemical and biophysical study over the past half century (????). A recent work (?) ex-  
 253     amined the respiratory capacity of the *E. coli* electron transport complexes using structural and  
 254     biochemical data, revealing that each electron transport chain rapidly pumps protons into the in-  
 255     termembrane space at a clip of  $\approx 1500$  protons per second (BIND: 114704; 114687, ?). Using our  
 256     estimate of the number of ATP synthases required per cell (**Figure 4(A)**), coupled with these re-  
 257     cent measurements, we estimate that  $\approx 1000$  electron transport complexes would be necessary to  
 258     facilitate the  $\approx 4 \times 10^6$  protons per second diet of the cellular ATP synthases. This estimate is in  
 259     agreement with the number of complexes identified in the proteomic datasets (plot in **Figure 4(B)**).

### 260     Energy Production in a Crowded Membrane.

261     For each protein considered so far, the data shows that in general their numbers increase with  
 262     growth rate. This is in part a consequence of the increase in cell length and width at that is com-  
 263     mon to many rod-shaped bacteria at faster growth rates (??). For the particular case of *E. coli*, the  
 264     total cellular protein and cell size increase logarithmically with growth rate (??). Indeed, this is one  
 265     reason why we have considered only a single, common growth condition across all our estimates  
 266     so far. Such a scaling will require that the total number of proteins and net demand on resources  
 267     also grow in proportion to the increase in cell size divided by the cell's doubling time. Recall how-  
 268     ever that each transport process, as well as the ATP production via respiration, is performed at the

**269** bacterial membrane. This means that their maximum productivity can only increase in proportion  
**270** to the cell's surface area divided by the cell doubling time. This difference in scaling would vary in  
**271** proportion to the surface area-to-volume (S/V) ratio.

**272** While we found that there was more than sufficient membrane real estate for carbon intake in  
**273** our earlier estimate, the total number of ATP synthases and electron chain transport complexes  
**274** both exhibit a clear increase in copy number with growth rate, reaching in excess of  $10^4$  copies per  
**275** cell (**Figure 4**). Here we consider the consequences of this S/V ratio scaling in more detail.

**276** In our estimate of ATP production above we found that a cell demands about  $6 \times 10^9$  ATP or  $10^6$   
**277** ATP/s. With a cell volume of roughly 1 fL, this corresponds to about  $2 \times 10^{10}$  ATP per fL of cell volume,  
**278** in line with previous estimates (??). In **Figure 5** (A) we plot this ATP demand as a function of the  
**279** S/V ratio in green, where we have considered a range of cell shapes from spherical to rod-shaped  
**280** with an aspect ratio (length/width) equal to 4 (See appendix for calculations of cell volume and  
**281** surface area). In order to consider the maximum power that could be produced, we consider the  
**282** amount of ATP that can be generated by a membrane filled with ATP synthase and electron transport  
**283** complexes, which provides a maximal production of about 3 ATP / (nm<sup>2</sup>·s) (?). This is shown in  
**284** red in **Figure 5**(A), which shows that at least for the growth rates observed, the energy demand is  
**285** roughly an order of magnitude less. Interestingly, ? also found that ATP production by respiration  
**286** is less efficient than by fermentation per membrane area occupied due to the additional proteins  
**287** of the electron transport chain. This suggests that even under anaerobic growth, there will be  
**288** sufficient membrane space for ATP production in general.

**289** While this serves to highlight the diminishing capacity to provide resources to grow if the cell  
**290** increases in size (and its S/V decreases), the blue region in **Figure 5**(A) represents a somewhat un-  
**291** achievable limit since the inner membrane must also include other proteins such as those required  
**292** for lipid and membrane synthesis. To gain insight, we used the proteomic data to look at the distri-  
**293** bution of proteins on the inner membrane. Here we use Gene Ontology (GO) annotations (??) to  
**294** identify all proteins embedded or peripheral to the inner membrane (GO term: 0005886). Those  
**295** associated but not membrane-bound include proteins like MreB and FtsZ, that traverse the inner  
**296** membrane by treadmilling and must nonetheless be considered as a vital component occupying  
**297** space on the membrane. In **Figure 5** (B), we find that the total protein mass per  $\mu\text{m}^2$  is relatively  
**298** constant with growth rate. Interestingly, when we consider the distribution of proteins grouped  
**299** by their Clusters of Orthologous Groups (COG) (?), the relative abundance for those in metabolism  
**300** (including ATP synthesis via respiration) is also relatively constant.

### **301** Function of the Central Dogma

**302** Up to this point, we have considered a variety of transport and biosynthetic processes that are  
**303** critical to acquiring and generating new cell mass. While there are of course many other metabolic  
**304** processes we could consider and perform estimates of (such as the components of fermentative  
**305** versus aerobic respiration), we now turn our focus to some of the most central processes which  
**306** *must* be undertaken irrespective of the growth conditions – the processes of the central dogma.

### **307** DNA

**308** Most bacteria (including *E. coli*) harbor a single, circular chromosome and can have extra-chromosomal  
**309** plasmids up to ~ 100 kbp in length. We will focus our quantitative thinking solely on the chromo-  
**310** some of *E. coli* which harbors ≈ 5000 genes and ≈  $5 \times 10^6$  base pairs. To successfully divide and  
**311** produce viable progeny, this chromosome must be faithfully replicated and segregated into each  
**312** nascent cell. We again rely on the near century of literature in molecular biology to provide some  
**313** insight on the rates and mechanics of the replicative feat as well as the production of the required  
**314** starting materials, dNTPs.

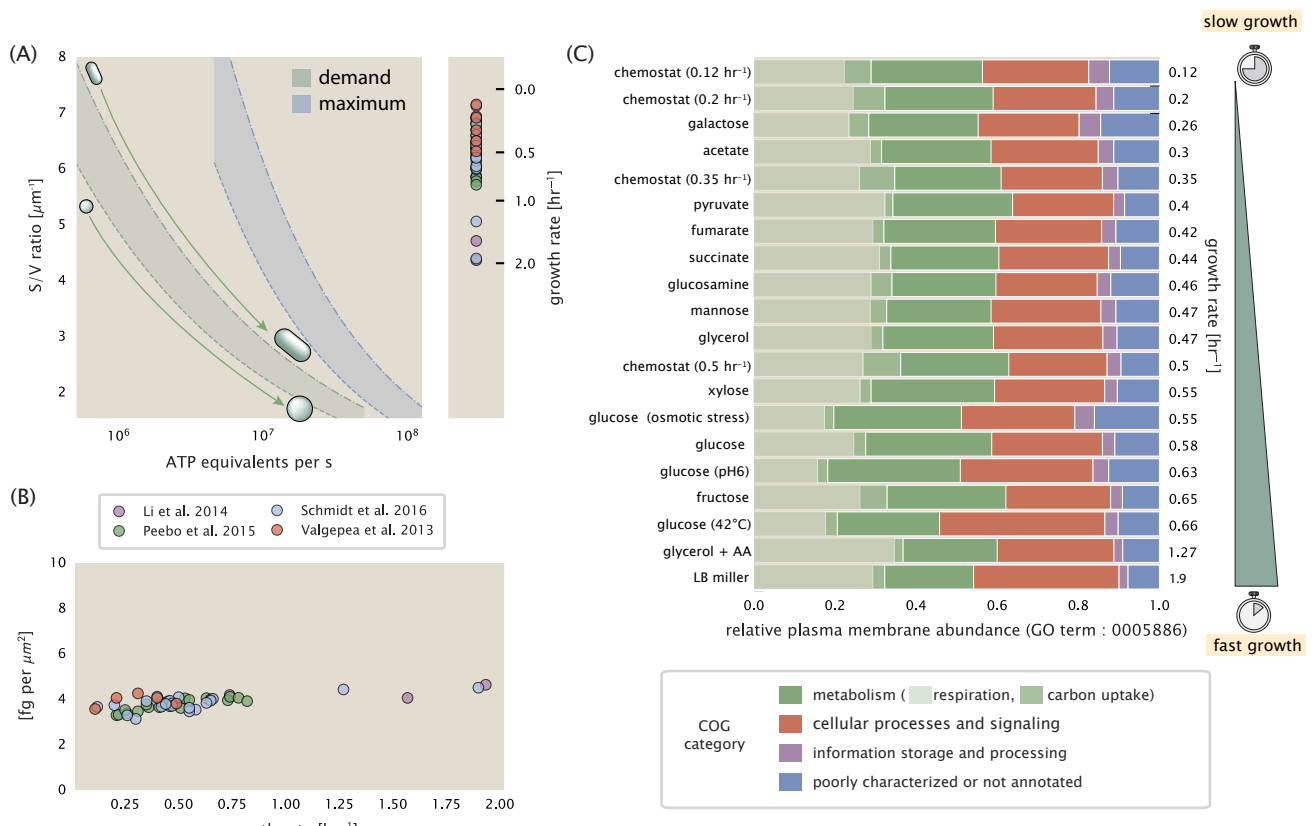


**Figure 5. Influence of cell size and S/V ratio on ATP production and inner membrane composition.** (A) Scaling of ATP demand and maximum ATP production as a function of S/V ratio. Cell volumes of 0.5 fL to 50 fL were considered, with the dashed (—) line corresponding to a sphere and the dash-dot line (---) reflecting a rod-shaped bacterium like *E. coli* with aspect ratio (length / width) of 0.4. Approximately 50% of the bacterial inner membrane is assumed to be protein, with the remainder lipid. (B) Total protein mass calculated for proteins with inner membrane annotation (GO term: 0005886). (C) Relative protein abundances by mass based on COG annotation. Metabolic proteins are further separated into respiration ( $F_1$ - $F_0$  ATP synthase, NADH dehydrogenase I, succinate:quinone oxidoreductase, cytochrome bo<sub>3</sub> ubiquinol oxidase, cytochrome bd-I ubiquinol oxidase) and carbohydrate transport (GO term: GO:0008643). Note that the elongation factor EF-Tu can also associate with the inner membrane, but was excluded in this analysis due to its high relative abundance (roughly identical to the total mass shown in part (B)).

315 dNTP synthesis

316 We begin our exploration DNA replication by examining the production of the deoxyribonucleotide  
 317 triphosphates (dNTPs). The four major dNTPs (dATP, dTTP, dCTP, and dGTP) are synthesized *de*  
 318 *novo* in separate pathways, requiring different building blocks. However, a critical step present  
 319 in all dNTP synthesis pathways is the conversion from ribonucleotide to deoxyribonucleotide via  
 320 the removal of the 3' hydroxyl group of the ribose ring (?). This reaction is mediated by a class of  
 321 enzymes termed ribonucleotide reductases, of which *E. coli* possesses two aerobically active com-  
 322 plexes (termed I and II) and a single anaerobically active enzyme. Due to their peculiar formation  
 323 of a radical intermediate, these enzymes have received much biochemical, kinetic, and structural  
 324 characterization. One such work (?) performed a detailed *in vitro* measurement of the steady-state  
 325 kinetic rates of these complexes, revealing a turnover rate of  $\approx 10$  dNTP per second.

326 Since this reaction is central to the synthesis of all dNTPs, it is reasonable to consider the abun-  
 327 dance of these complexes is a measure of the total dNTP production in *E. coli*. Illustrated schemati-  
 328 cally in **Figure 6** (A), we consider the fact that to replicate the cell's genome, on the order of  $\approx 10^7$   
 329 dNTPs must be synthesized. Assuming a production rate of 10 per second per ribonucleotide  
 330 reductase complex and a cell division time of 6000 seconds, we arrive at an estimate of  $\approx 150$  com-  
 331 plexes needed per cell. As shown in the bottom panel of **Figure 6** (A), this estimate agrees with the  
 332 experimental measurements of these complexes abundances within  $\approx 1/2$  an order of magnitude.

333 Recent work has revealed that during replication, the ribonucleotide reductase complexes co-  
 334 alesce to form discrete foci colocalized with the DNA replisome complex (?). This is particularly  
 335 pronounced in conditions where growth is slow, indicating that spatial organization and regula-  
 336 tion of the activity of the complexes plays an important role.

337 DNA Replication

338 We now turn our focus to the integration of these dNTP building blocks into the replicated chromo-  
 339 some strand via the DNA polymerase. Replication is initiated at a single region of the chromosome  
 340 termed the *oriC* locus at which a pair of DNA polymerases bind and begin their high-fidelity repli-  
 341 cation of the genome in opposite directions. Assuming equivalence between the two replication  
 342 forks, this means that the two DNA polymerase complexes (termed replisomes) meet at the mid-  
 343 way point of the circular chromosome termed the *ter* locus. The kinetics of the five types of DNA  
 344 polymerases (I – V) have been intensely studied, revealing that DNA Polymerase III performs the  
 345 high fidelity processive replication of the genome with the other "accessory" polymerases playing  
 346 auxiliary roles (?). *In vitro* measurements have shown that DNA Polymerase III copies DNA at a rate  
 347 of  $\approx 600$  nucleotides per second (BNID: 104120, ?). Therefore, to replicate a single chromosome,  
 348 two replisomes moving at their maximal rate would copy the entire genome in  $\approx 4000$  s. Thus, with  
 349 a division time of 5000 s (our "typical" growth rate for the purposes of this work), there is sufficient  
 350 time for a pair of DNA polymerase III complexes to replicate the entire genome. However, this  
 351 estimate implies that 4000 s would be the upper-limit time scale for bacterial division which is at  
 352 odds with the familiar 20 minute (1200 s) doubling time of *E. coli* in rich medium.

353 It is well known that *E. coli* can parallelize its DNA replication such that multiple chromosomes  
 354 are being replicated at once, with as many as 10 - 12 replication forks at a given time (??). Thus,  
 355 even in rapidly growing cultures, we expect only a few polymerases ( $\approx 10$ ) are needed to repli-  
 356 cate the chromosome per cell doubling. However, as shown in **Figure 6(B)**, DNA polymerase III  
 357 is nearly an order of magnitude more abundant. This discrepancy can be understood  
 358 by considering its binding constant to DNA. DNA polymerase III is highly processive, facilitated by  
 359 a strong affinity of the complex to the DNA. *In vitro* biochemical characterization has quantified  
 360 the  $K_D$  of DNA polymerase III holoenzyme to single-stranded and double-stranded DNA to be 50  
 361 and 200 nM, respectively (?). The bottom plot in **Figure 6** (B) shows that the concentration of the  
 362 DNA polymerase III across all data sets and growth conditions is within this range. Thus, while the  
 363 copy number of the DNA polymerase III is in excess of the strict number required to replicate the  
 364 genome, its copy number appears to vary such that its concentration is approximately equal to the

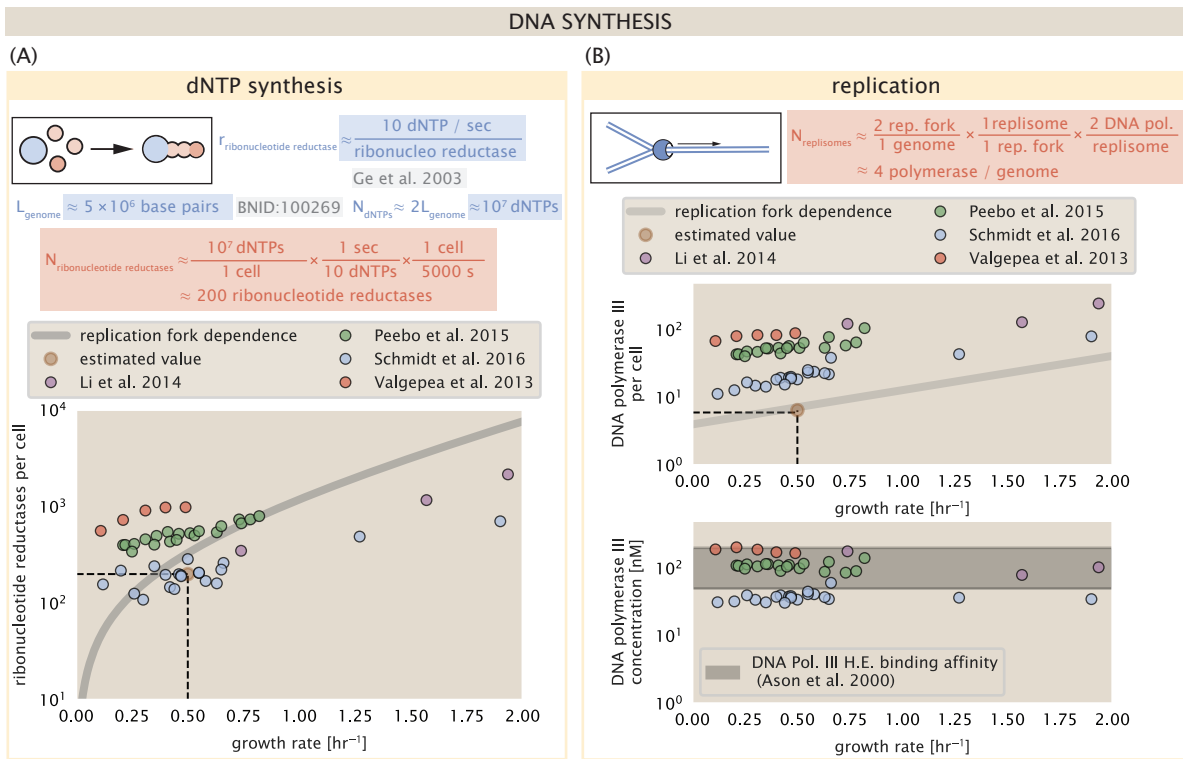


**Figure 6. Complex abundance estimates for dNTP synthesis and DNA replication.** (A) Estimate of the number of ribonucleotide reductase enzymes needed to facilitate the synthesis of  $\approx 10^7$  dNTPs over the course of a 6000 second generation time. Points in the plot correspond to the total number of ribonucleotide reductase I ( $[\text{NrdA}]_2[\text{NrdB}]_2$ ) and ribonucleotide reductase II ( $[\text{NrdE}]_2[\text{NrdF}]_2$ ) complexes. (B) An estimate for the minimum number of DNA polymerase holoenzyme complexes needed to facilitate replication of a single genome. Points in the top plot correspond to the total number of DNA polymerase III holoenzyme complexes ( $[\text{DnaE}]_3[\text{DnaQ}]_3[\text{HolE}]_3[\text{DnaX}]_5[\text{HolB}][\text{HolA}][\text{DnaN}]_4[\text{HolC}]_4[\text{HolD}]_4$ ) per cell. Bottom plot shows the effective concentration of DNA polymerase III holoenzyme given cell volumes calculated from the growth rate as in ? (See Appendix Section 4).

365 dissociation constant to the DNA. While the processes regulating the initiation of DNA replication  
 366 are complex and involve more than just the holoenzyme, these data indicate that the kinetics of  
 367 replication rather than the explicit copy number of the DNA polymerase III holoenzyme is the more  
 368 relevant feature of DNA replication to consider. In light of this, the data in **Figure 6(B)** suggests that  
 369 for bacteria like *E. coli*, DNA replication does no that represent a rate-limiting step in cell division.  
 370 However, it is worth noting that for bacterium like *C. crescentus* whose chromosomal replication  
 371 is initiated only once per cell cycle (?), the time to double their chromosome likely represents an  
 372 upper limit to their growth rate.

### 373 RNA Synthesis

374 With the machinery governing the replication of the genome accounted for, we now turn our attention  
 375 to the next stage of the central dogma – the transcription of DNA to form RNA. We primarily  
 376 consider three major groupings of RNA, namely the RNA associated with ribosomes (rRNA), the  
 377 RNA encoding the amino-acid sequence of proteins (mRNA), and the RNA which links codon sequence  
 378 to amino-acid identity during translation (tRNA). Despite the varied function of these RNA species,  
 379 they share a commonality in that they are transcribed from DNA via the action of RNA polymerase. In the coming paragraphs, we will consider the synthesis of RNA as a rate limiting  
 380 step in bacterial division by estimating how many RNA polymerases must be present to synthesize  
 381 all necessary rRNA, mRNA, and tRNA.

### 383 rRNA

384 We begin with an estimation of the number of RNA polymerases needed to synthesize the rRNA  
 385 that serve as catalytic and structural elements of the ribosome. Each ribosome contains three rRNA  
 386 molecules of lengths 120, 1542, and 2904 nucleotides (BNID: 108093, ?), meaning each ribosome  
 387 contains  $\approx 4500$  nucleotides. As the *E. coli* RNA polymerase transcribes DNA to RNA at a rate of  $\approx$   
 388 40 nucleotides per second (BNID: 101904, ?), it takes a single RNA polymerase  $\approx 100$  s to synthesize  
 389 the RNA needed to form a single functional ribosome. Therefore, in a 5000 s division time, a single  
 390 RNA polymerase transcribing rRNA at a time would result in only  $\approx 50$  functional ribosomal rRNA  
 391 units – far below the observed number of  $\approx 10^4$  ribosomes per cell.

392 Of course, there can be more than one RNA polymerase transcribing the rRNA genes at any  
 393 given time. To elucidate the *maximum* number of rRNA units that can be synthesized given a single  
 394 copy of each rRNA gene, we will consider a hypothesis in which the rRNA operon is completely tiled  
 395 with RNA polymerase. *In vivo* measurements of the kinetics of rRNA transcription have revealed  
 396 that RNA polymerases are loaded onto the promoter of an rRNA gene at a rate of  $\approx 1$  per second  
 397 (BNID: 111997; 102362, ?). If RNA polymerases are being constantly loaded on to the rRNA genes  
 398 at this rate, then we can assume that  $\approx 1$  functional rRNA unit is synthesized per second. With a  
 399 5000 second division time, this hypothesis leads to a maximal value of 5000 functional rRNA units,  
 400 still undershooting the observed number of  $10^4$  ribosomes per cell.

401 *E. coli* has evolved a clever mechanism to surpass this kinetic limit for the rate of rRNA production.  
 402 Rather than having only one copy of each rRNA gene, *E. coli* has seven copies of the operon  
 403 (BIND: 100352, ?) four of which are localized directly adjacent to the origin of replication (?). As fast  
 404 growth also implies an increased gene dosage due to paralellized chromosomal replication, the total  
 405 number of rRNA genes can be on the order of  $\approx 10 - 70$  copies at moderate to fast growth rates  
 406 (?). Using our standard time scale of a 5000 second division time, we can make the lower-bound  
 407 estimate that the typical cell will have 7 copies of the rRNA operon. Synthesizing one functional  
 408 rRNA unit per second per rRNA operon, a total of  $4 \times 10^4$  rRNA units can be synthesized, comfortably  
 409 above the observed number of ribosomes per cell.

410 How many RNA polymerases are then needed to constantly transcribe 7 copies of the rRNA  
 411 genes? We approach this estimate by considering the maximum number of RNA polymerases tiled  
 412 along the rRNA genes with a loading rate of 1 per second and a transcription rate of 40 nucleotides  
 413 per second. Considering that a RNA polymerase has a physical footprint of approximately 40 nu-

**414** cleotides (BNID: 107873, ?), we can expect  $\approx 1$  RNA polymerase per 80 nucleotides. With a total  
**415** length of  $\approx 4500$  nucleotides per operon and 7 operons per cell, the maximum number of RNA  
**416** polymerases that can be transcribing rRNA at any given time is  $\approx 400$ . As we will see in the coming  
**417** sections, the synthesis of rRNA is the dominant requirement of the RNA polymerase pool.

**418** mRNA

**419** To form a functional protein, all protein coding genes must first be transcribed from DNA to form an  
**420** mRNA molecule. While each protein requires an mRNA blueprint, many copies of the protein can  
**421** be synthesized from a single mRNA. Factors such as strength of the ribosomal binding site, mRNA  
**422** stability, and rare codon usage frequency dictate the number of proteins that can be made from  
**423** a single mRNA, with yields ranging from  $10^1$  to  $10^4$  (BNID: 104186; 100196; 106254, ?). Computing  
**424** the geometric mean of this range yields  $\approx 1000$  proteins synthesized per mRNA, a value that agrees  
**425** with experimental measurements of the number of proteins per cell ( $\approx 3 \times 10^6$ , BNID: 100088, ?)  
**426** and total number of mRNA per cell ( $\approx 3 \times 10^3$ , BNID: 100064, ?).

**427** This estimation captures the *steady-state* mRNA copy number, meaning that at any given time,  
**428** there will exist approximately 3000 unique mRNA molecules. To determine the *total* number of  
**429** mRNA that need to be synthesized over the cell's lifetime, we must consider degradation of the  
**430** mRNA. In most bacteria, mRNAs are rather unstable with life times on the order of several minutes  
**431** (BNID: 104324; 106253; 111927; 111998, ?). For convenience, we assume that the typical mRNA in  
**432** our cell of interest has a typical lifetime of  $\approx 300$  seconds. Using this value, we can determine  
**433** the total mRNA production rate to maintain a steady-state copy number of 3000 mRNA per cell.  
**434** While we direct the reader to the appendix for a more detailed discussion of mRNA transcriptional  
**435** dynamics, we state here that the total mRNA production rate must be on the order of  $\approx 15$  mRNA  
**436** per second. In *E. coli*, the average protein is  $\approx 300$  amino acids in length (BNID: 108986; ?), meaning  
**437** that the corresponding mRNA is  $\approx 900$  nucleotides which we will further approximate as  $\approx 1000$   
**438** nucleotides to account for the non-protein coding regions on the 5' and 3' ends. This means that  
**439** the cell must have enough RNA polymerase molecules about to sustain a transcription rate of  
**440**  $\approx 1.5 \times 10^4$  nucleotides per second. Knowing that a single RNA polymerase polymerizes RNA at a  
**441** clip of 40 nucleotides per second, we arrive at a comfortable estimate of  $\approx 250$  RNA polymerase  
**442** complexes needed to satisfy the mRNA demands of the cell. It is worth noting that this number is  
**443** approximately half of that required to synthesize enough rRNA, as we saw in the previous section.  
**444** We find this to be a striking result as these 250 RNA polymerase molecules are responsible for the  
**445** transcription of the  $\approx 4000$  protein coding genes that are not ribosome associated.

**446** tRNA

**447** The final class of RNA molecules worthy of quantitative consideration is the the pool of tRNAs  
**448** used during translation to map codon sequence to amino acid identity. Unlike mRNA or rRNA,  
**449** each individual tRNA is remarkably short, ranging from 70 to 95 nucleotides each (BNID: 109645;  
**450** 102340, ?). What they lack in length, they make up for in abundance. There are approximately  
**451**  $\approx 3000$  tRNA molecules present for each of the 20 amino acids (BNID: 105280, ?), although the  
**452** precise copy number is dependent on the identity of the ligated amino acid. Using these values,  
**453** we make the estimate that  $\approx 5 \times 10^6$  nucleotides are sequestered in tRNA per cell. Unlike mRNA,  
**454** tRNA is remarkably stable with typical lifetimes *in vivo* on the order of  $\approx 48$  hours (??) – well beyond  
**455** the timescale of division. Once again using our rule-of-thumb for the rate of transcription to be 40  
**456** nucleotides per second and assuming a division time of  $\approx 5000$  seconds, we arrive at an estimate  
**457** of  $\approx 20$  RNA polymerases to synthesize enough tRNA. This requirement pales in comparison to the  
**458** number of polymerases needed to generate the rRNA and mRNA pools and can be neglected as a  
**459** significant transcriptional burden.

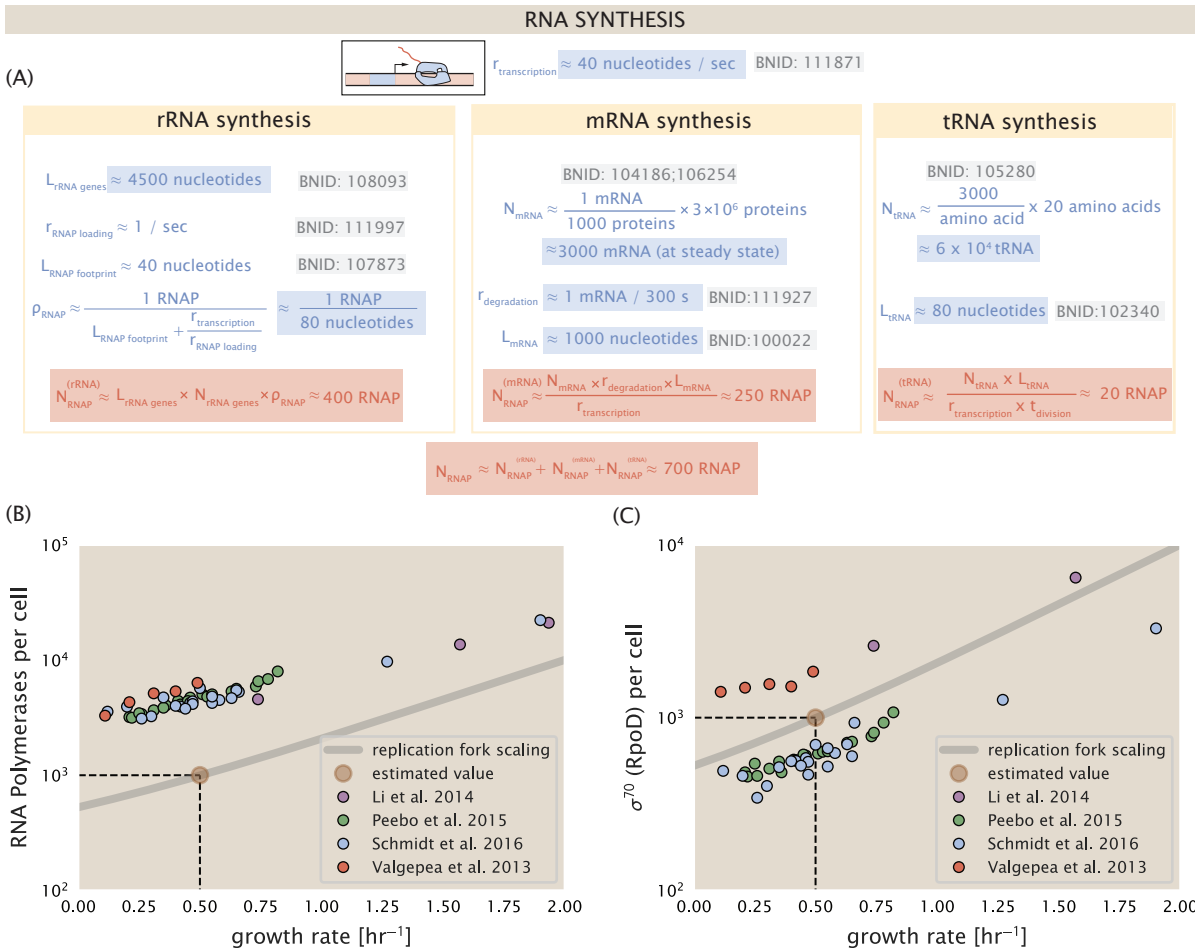


**Figure 7. Estimation of the RNA polymerase demand and comparison with experimental data.** (A) Estimations for the number of RNA polymerase needed to synthesize sufficient quantities of rRNA, mRNA, and tRNA from left to right, respectively. Bionumber Identifiers (BNIDs) are provided for key quantities used in the estimates. (B) The RNA polymerase core enzyme copy number as a function of growth rate. Colored points correspond to the average number RNA polymerase core enzymes that could be formed given a subunit stoichiometry of  $[RpoA]_2[RpoC][RpoB]$ . (C) The abundance of  $\sigma^{70}$  as a function of growth rate. Estimated value for the number of RNAP is shown in (B) and (C) as a translucent brown point at a growth rate of  $0.5 \text{ hr}^{-1}$ .

**460 RNA Polymerase and  $\sigma$ -factor Abundance**

461 These estimates, summarized in **Figure 7 (A)**, reveal that synthesis of rRNA and mRNA are the domi-  
 462 nant RNA species synthesized by RNA polymerase, suggesting the need for  $\approx 700$  RNA polymerases  
 463 per cell. As is revealed in **Figure 7 (B)**, this estimate is about an order of magnitude below the ob-  
 464 served number of RNA polymerase complexes per cell ( $\approx 5000 - 7000$ ). The disagreement between  
 465 the estimated number of RNA polymerases and these observations are at least consistent with  
 466 recent literature revealing that  $\approx 80\%$  of RNA polymerases in *E. coli* are not transcriptionally active  
 467 (?). Our estimate ignores the possibility that some fraction is only nonspecifically bound to DNA,  
 468 as well as the obstacles that RNA polymerase and DNA polymerase present for each other as they  
 469 move along the DNA (?).

470 In addition, it is also vital to consider the role of  $\sigma$ -factors which help RNA polymerase iden-  
 471 tify and bind to transcriptional start sites (?). Here we consider  $\sigma^{70}$  (RpoD) which is the dominant  
 472 "general-purpose"  $\sigma$ -factor in *E. coli*. While initially thought of as being solely involved in transcrip-  
 473 tional initiation, the past two decades of single-molecule work has revealed a more multipurpose  
 474 role for  $\sigma^{70}$  including facilitating transcriptional elongation (?????). **Figure 7 (B)** is suggestive of such  
 475 a role as the number of  $\sigma^{70}$  proteins per cell is in close agreement with our estimate of the number  
 476 of transcriptional complexes needed.

477 While these estimates and comparison with experimental data reveal an interesting dynamic  
 478 at play between the transcriptional demand and copy numbers of the corresponding machinery,  
 479 these findings illustrate that transcription cannot be the rate limiting step in bacterial division. **Fig-**  
 480 **ure 7 (A)** reveals that the availability of RNA polymerase is not a limiting factor for cell division as the  
 481 cell always has an apparent  $\sim 10$ -fold excess than needed. Furthermore, if more transcriptional  
 482 activity was needed to satisfy the cellular requirements, more  $\sigma^{70}$ -factors could be expressed to  
 483 utilize a larger fraction of the RNA polymerase pool.

**484 Translation and ribosomal synthesis**

485 Lastly, we turn our attention to the process of synthesizing new proteins, translation. These pro-  
 486 cesses stand as good candidates for defining the growth limit as the synthesis of new proteins  
 487 relies on the generation of ribosomes, themselves proteinaceous molecules. As we will see in the  
 488 coming sections of this work, this poses a "chicken-or-the-egg" problem where the synthesis of  
 489 ribosomes requires ribosomes in the first place.

490 We will begin our exploration of protein translation in the same spirit as we have in previous  
 491 sections – we will draw order-of-magnitude estimates based on our intuition and relying on litera-  
 492 ture studies and will compare these estimates to the observed data. In doing so, we will estimate  
 493 both the absolute number of ribosomes necessary for replication of the proteome as well as the  
 494 synthesis of amino-acyl tRNAs. In the closing sections, we will explore the details of ribosome bio-  
 495 genesis in granular detail, ultimately presenting a quantitative model tying ribosome abundance  
 496 to the concentration of amino acids as well as the state of chromosome replication.

**497 tRNA synthetases**

498 We begin by first estimating the number of tRNA ligases in *E. coli* needed to convert free amino-  
 499 acids to polypeptide chains. At a modest growth rate of  $\approx 5000$  s, *E. coli* has roughly  $3 \times 10^6$  proteins  
 500 per cell (BNID: 115702; ?). Assuming that the typical protein is on the order of  $\approx 300$  amino acids  
 501 in length (BNID: 100017; ?), we can estimate that a total of  $\approx 10^9$  amino acids are stitched together  
 502 by peptide bonds.

503 How many tRNAs are needed to facilitate this remarkable number of amino acid delivery events  
 504 to the translating ribosomes? It is important to note that tRNAs are recycled after they've passed  
 505 through the ribosome and can be recharged with a new amino acid, ready for another round of  
 506 peptide bond formation. While some *in vitro* data exists on the turnover of tRNA in *E. coli* for  
 507 different amino acids, we can make a reasonable estimate by comparing the number of amino  
 508 acids to be polymerized to cell division time. Using our stopwatch of 5000 s and  $10^9$  amino acids,

**509** we arrive at a requirement of  $\approx 2 \times 10^5$  tRNA molecules. This estimate is in line with experimental  
**510** measurements of  $\approx 3 \times 10^5$  per cell (BNID: 108611, ?), suggesting we are on the right track.

**511** There are many processes which go into synthesizing a tRNA and ligating it with the appropriate  
**512** amino acids. As we covered in the previous section, there appear to be more than enough RNA  
**513** polymerases per cell to synthesize the needed pool of tRNAs. Without considering the many ways  
**514** in which amino acids can be scavenged or synthesized *de novo*, we can explore ligation as a potential  
**515** rate limiting step. The enzymes which link the correct amino acid to the tRNA, known  
**516** as tRNA synthetases or tRNA ligases, are incredible in their proofreading of substrates with the  
**517** incorrect amino acid being ligated once out of every  $10^4$  to  $10^5$  times (BNID: 103469, ?). This is due  
**518** in part to the consumption of energy as well as a multi-step pathway to ligation. While the rate  
**519** at which tRNA is ligated is highly dependent on the identity of the amino acid, it is reasonable to  
**520** state that the typical tRNA synthetase has charging rate of  $\approx 20$  AA per tRNA synthetase per second  
**521** (BNID: 105279, ?).

**522** Combining these estimates together, as shown schematically in *Figure 8(A)*, yields an estimate  
**523** of  $\approx 10^4$  tRNA synthetases per cell with a division time of 5000 s. This point estimate is in very close  
**524** agreement with the observed number of synthetases (the sum of all 20 tRNA synthetases in *E. coli*).  
**525** This estimation strategy seems to adequately describe the observed growth rate dependence of  
**526** the tRNA synthetase copy number (shown as the grey line in *Figure 8(B)*), suggesting that the copy  
**527** number scales with the cell volume.

**528** In total, the estimated and observed  $\approx 10^4$  tRNA synthetases occupy only a meager fraction of  
**529** the total cell proteome, around 0.5% by abundance. It is reasonable to assume that if tRNA charging  
**530** was a rate limiting process, cells would be able to increase their growth rate by devoting more  
**531** cellular resources to making more tRNA synthases. As the synthesis of tRNAs and the corresponding  
**532** charging can be highly parallelized, we can argue that tRNA charging is not a rate limiting step  
**533** in cell division, at least for the growth conditions explored in this work.

#### **534** Protein synthesis

**535** With the number of tRNA synthetases accounted for, we now consider the abundance of the protein  
**536** synthesis machines themselves, ribosomes. Ribosomes are enormous protein/rRNA complexes  
**537** that facilitate the peptide bond formation between amino acids in the correct sequence  
**538** as defined by the coding mRNA. Before we examine the synthesis of the ribosome proteins and  
**539** the limits that may place on the observed bacterial growth rates, let's consider replication of the  
**540** cellular proteome.

**541** As described in the previous section, *E. coli* consists of  $\approx 3 \times 10^6$  proteins at a growth rate of  $\approx$   
**542** 5000 s. If we again assume that each protein is composed of  $\approx 300$  amino acids and each amino  
**543** acid is linked together by one peptide bond, we arrive at an estimate that the cellular proteome  
**544** consists of  $\approx 10^{10}$  peptide bonds. While the rate at which ribosomes translates is well known to  
**545** have a growth rate dependence ? and is a topic which we discuss in detail in the coming sections.  
**546** However, for the purposes of our order-of-magnitude estimate, we can make the approximation  
**547** that translation occurs at a rate of  $\approx 15$  amino acids per second per ribosome (BNID: 100233, ?).  
**548** Under this approximation and assuming a division time of 5000 s, we can arrive at an estimate  
**549** of  $\approx 10^4$  ribosomes are needed to replicate the cellular proteome, shown in *Figure 8(B)*. This point  
**550** estimate, while glossing over important details such as chromosome copy number and growth-rate  
**551** dependent translation rates, proves to be notably accurate when compared to the experimental  
**552** observations (*Figure 8(B)*).

#### **553** Translation as a growth-rate limiting step

**554** Thus far in our work, the general back-of-the-envelope estimates have been reasonably successful  
**555** in explaining what sets the scale of absolute protein copy number. In many cases, these estimates  
**556** can be adapted to consider a continuum of growth rates in lieu of a single 5000 s point estimate,  
**557** the details of which are described in the Supplemental Information. A recurring theme we have

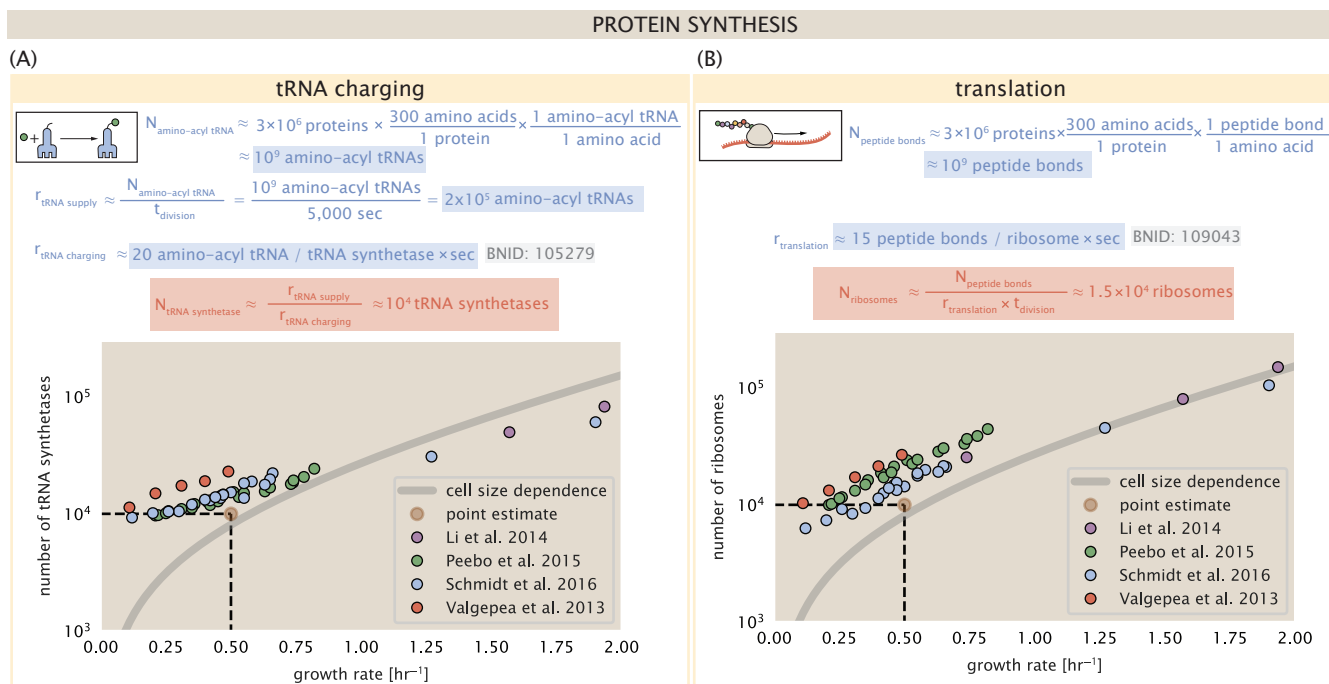


**Figure 8. Estimation of the required tRNA synthetases and ribosomes.** (A) Estimation for the number of tRNA synthetases that will supply the required amino acid demand. The sum of all tRNA synthetases copy numbers are plotted as a function of growth rate ([ArgS], [CysS], [GlnS], [Glx], [IleS], [LeuS], [ValS], [AlaS]<sub>2</sub>, [AsnS]<sub>2</sub>, [AspS]<sub>2</sub>, [TyrS]<sub>2</sub>, [TrpS]<sub>2</sub>, [ThrS]<sub>2</sub>, [SerS]<sub>2</sub>, [ProS]<sub>2</sub>, [PheS]<sub>2</sub>[PheT]<sub>2</sub>, [MetG]<sub>2</sub>, [LysS]<sub>2</sub>, [GlyS]<sub>2</sub>[GlyQ]<sub>2</sub>). (B) Estimation of the number of ribosomes required to synthesize 10<sup>9</sup> peptide bonds with an elongation rate of 15 peptide bonds per second. The average abundance of ribosomes is plotted as a function of growth rate. Our estimated values are shown for a growth rate of 0.5 hr<sup>-1</sup>. Grey lines correspond to the estimated complex abundance calculated at different growth rates. See Supplemental Information XX for a more detail description of this calculation.

558 relied on is the ability of the cell to parallelize different processes to transport or synthesize the  
559 required amount of the corresponding biomolecule. For example, we saw in our example of *E. coli*  
560 grown on different carbon sources that expression of particular transporters can be induced, often  
561 producing more than needed acquire enough carbon to build new cell mass (??(B)). In examining  
562 replication of the DNA, we described how cells can replicate multiple copies of the chromosome  
563 at any given time, permitting growth rates faster than the limit at which the chromosome can be  
564 faithfully replicated. As a final example, we showed how increasing the gene dosage of the rRNA  
565 operons is necessary to produce enough rRNA to form functional ribosomes. However, when it  
566 comes to ribosome biogenesis, namely the translation of ribosomal proteins, such parallelization  
567 is not possible, suggesting that translation may be a key factor determining the cellular growth  
568 rate.

569 Optimal resource allocation and the role of ribosomal proteins have been an area of intense  
570 quantitative study over the last decade by Hwa and others (??). From the perspective of limiting  
571 growth, our earlier estimate of rRNA highlighted the necessity for multiple copies of rRNA genes in  
572 order to make enough rRNA. For *E. coli*'s fastest growth rates at 2 hr<sup>-1</sup>, the additional demand for  
573 rRNA is further supported by parallelized DNA replication and increased rRNA gene dosage. This  
574 suggests the possibility that synthesis of ribosomes might be rate limiting. While the transcrip-  
575 tional demand for the ribosomal proteins is substantially lower than rRNA genes, since proteins  
576 can be translated from relatively fewer mRNA, other ribosomal proteins like the translation elon-  
577 gation factor EF-Tu also present a substantial burden. For EF-Tu in particular, it is the most highly  
578 expressed protein in *E. coli* and is expressed from multiple gene copies, *tufA* and *tufB*.

579 To gain some intuition into how translation may set the speed limit for bacterial growth, we  
 580 again consider the total number of peptide bonds that must be synthesized,  $N_{AA}$ . Noting that cell  
 581 mass grows exponentially (?), we can compute the number of amino acids to be polymerized as

$$N_{AA} = \frac{r_t R}{\lambda}, \quad (1)$$

582 where  $\lambda$  is the cell growth rate in  $s^{-1}$ ,  $r_t$  is the maximum translation rate in amino acids per second,  
 583 and  $R$  is the average ribosome copy number per cell. Knowing the number of peptide boids to be  
 584 formed permits us to compute the translation-limited growth rate as

$$\lambda_{\text{translation-limited}} = \frac{r_t R}{N_{AA}}. \quad (2)$$

585 Alternatively, since  $N_{AA}$  is related to the total protein mass through the molecular weight of  
 586 each protein, we can also consider the growth rate in terms of the fraction of the total proteome  
 587 mass that is dedicated to ribosomal protein mass. By making the approximation that an average  
 588 amino acid has a molecular weight of 110 Da (see *Figure 9(A)*), we can rewrite the growth rate as,

$$\lambda_{\text{translation-limited}} \approx \frac{r_t}{L_R} \Phi_R, \quad (3)$$

589 where  $L_R$  is the total length in amino acids that make up a ribosome, and  $\Phi_R$  is the ribosomal mass  
 590 fraction. This is plotted as a function of ribosomal fraction  $\Phi_R$  in *Figure 9(A)*, where we take  $L_R \approx$   
 591 7500 aa, corresponding to the length in amino acids for all ribosomal subunits of the 50S and 30S  
 592 complex (BNID: 101175, (?)). This formulation assumes that the cell can transcribe the required  
 593 amount of rRNA, which appears reasonable for *E. coli*, allowing us to consider the inherent limit on  
 594 growth set by the ribosome.

595 The growth rate defined by Equation 3 reflects mass-balance under steady-state growth and  
 596 has long provided a rationalization to the apparent linear increase in *E. coli*'s ribosomal content  
 597 as a function of growth rate (??). For our purposes, there are several important consequences of  
 598 this trend. Firstly, we note there is a maximum growth rate of  $\lambda \approx 6hr^{-1}$ , or doubling time of about  
 599 7 minutes (dashed line). This growth rate can be viewed as an inherent maximum growth rate  
 600 due to the need for the cell to double the cell's entire ribosomal mass. Interestingly, this limit is  
 601 independent of the absolute number of ribosomes and is simply given by time to translate an entire  
 602 ribosome,  $L_R/r_t$ . As shown in *Figure 9(B)*, we can reconcile this with the observation that in order  
 603 to double the average number of ribosomes, each ribosome must produce a second ribosome.  
 604 Unlike DNA replication or rRNA transcription, this is a process that cannot be parallelized.

605 For reasonable values of  $\Phi_R$ , between about 0.1 - 0.3 (?), the maximum growth rate is in line with  
 606 experimentally reported growth rates around 0.5 - 2 hr $^{-1}$ . Importantly, in order for a cell to increase  
 607 their growth limit they *must* increase their relative ribosomal abundance. This can be achieved by  
 608 either synthesizing more ribosomes or reducing the fraction of non-ribosomal proteins. Reduction  
 609 of non-ribosomal proteins is not a straightforward task since (as we have found throughout our  
 610 estimates) doubling a cell requires many other enzymes and transporters. Increasing the absolute  
 611 ribosomal abundance in *E. coli* will be limited by the number of rRNA operons.

612 Here we again return to rRNA synthesis, but here consider the maximum rRNA that can be  
 613 produced at different growth rates.

614 [expand on.]

## 615 Discussion

616 [Fill in.]

### 617 Maximizing growth rate requires coordination of biosynthesis at all growth rates.

618 However, the mechanism behind growth rate control has remained elusive and has only been  
 619 described at a phenomenological level.

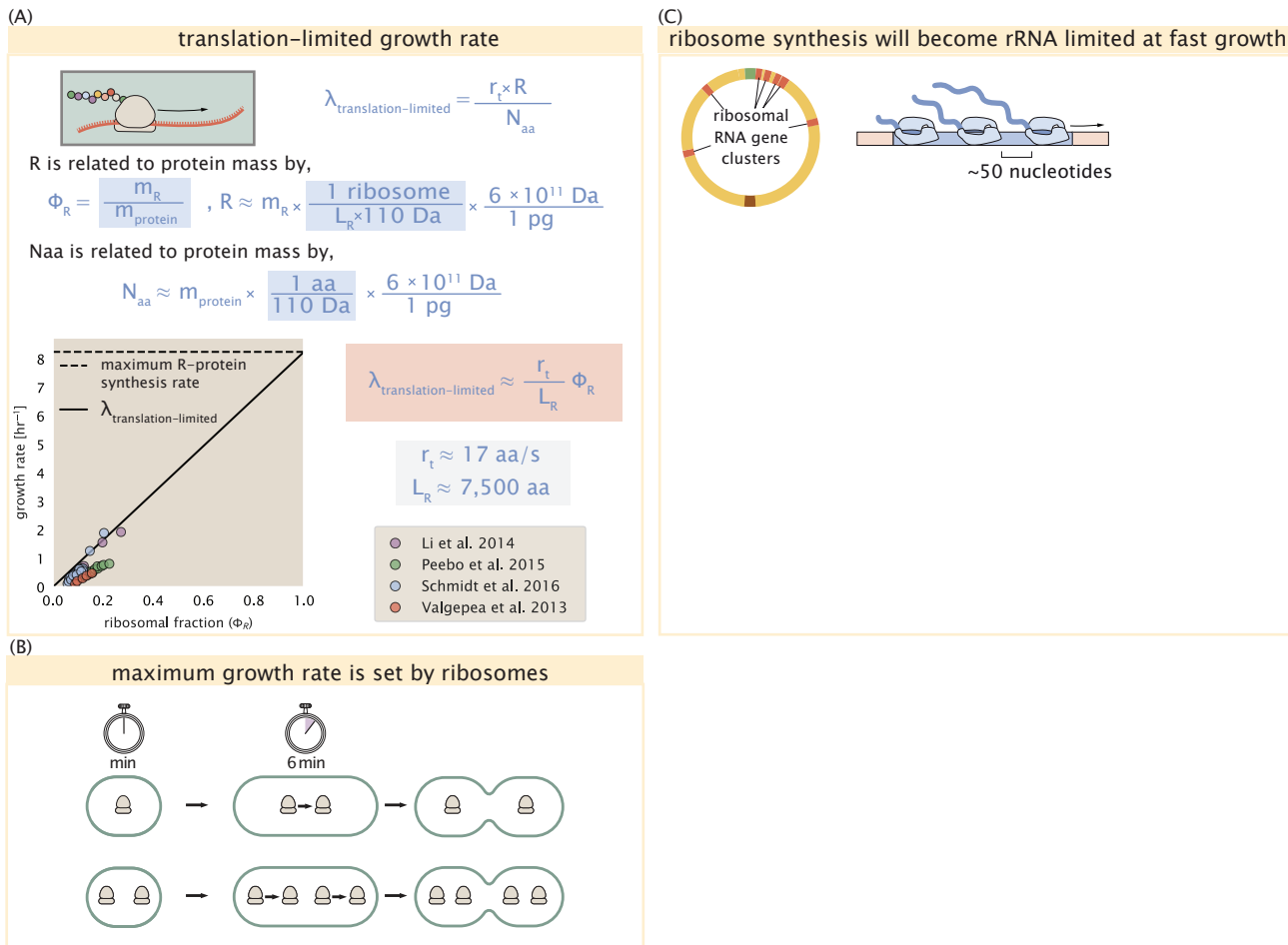


**Figure 9. Translation-limited growth rate.** (A) Here we consider the translation-limited growth as a function of ribosomal fraction. By mass balance, the time required to double the entire proteome ( $N_{AA} / r_t$ ) sets the translation-limited growth rate,  $\lambda_{\text{translation-limited}}$ . Here  $N_{aa}$  is effectively the number of peptide bonds that must be translated,  $r_t$  is the translation elongation rate, and  $R$  is the number of ribosomes. This can also be re-written in terms of the ribosomal mass fraction  $\Phi_R = m_R / m_{\text{protein}}$ , where  $m_R$  is the total ribosomal mass and  $m_{\text{protein}}$  is the mass of all proteins in the cell.  $L_R$  refers to the summed length of the ribosome in amino acids.  $\lambda_{\text{translation-limited}}$  is plotted as a function of  $\Phi_R$  (solid line). (B) The dashed line in part (A) identifies a maximum growth rate that is set by the ribosome. Specifically, this growth rate corresponds to the time required to translate an entire ribosome,  $L_R / r_t$ . This is a result that is independent of the number of ribosomes in the cell as shown schematically here. (C)

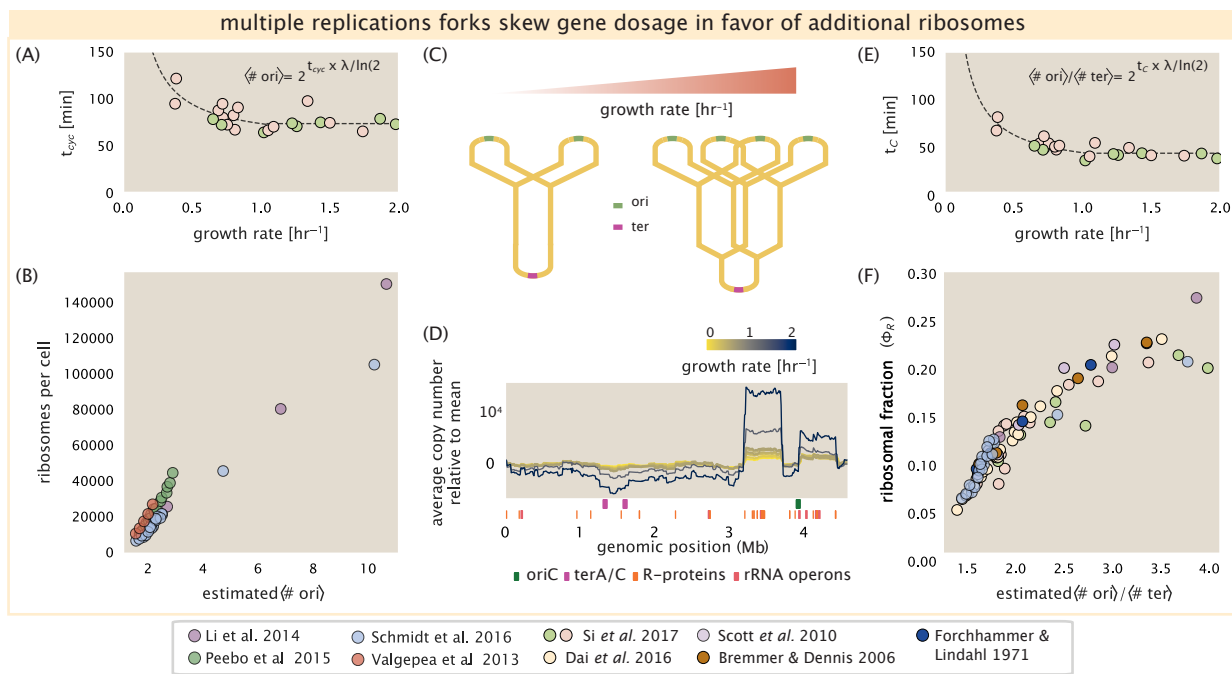


**Figure 10. Multiple replication forks skew gene dosage and ribosomal content.** (A) Schematic shows the expected increase in replication forks (or number of ori regions) as *E. coli* cells grow faster. (B) A running boxcar average of protein copy number is calculated for each each growth condition considered by Schmidt *et al.*. A 0.5 Mb averaging window was used. Protein copy numbers are reported relative to their condition-specific means in order to center all data sets. (C) and (E) show experimental data from Si *et al.* (2017) Solid lines show fits to the data, which were used to estimate  $\langle \# \text{ori} \rangle / \langle \# \text{ter} \rangle$  and  $\langle \# \text{ori} \rangle$  [NB: to note fit equations]. Red data points correspond to measurements in strain MG1655, while light green points are for strain NCM3722. (D) Plot compares our estimate of  $\langle \# \text{ori} \rangle / \langle \# \text{ter} \rangle$  to the experimental measurements of ribosomal abundance. Ribosomal fraction was approximated from the RNA/protein ratios of Dai *et al.* (2016) (yellow) and Si *et al.* (2017) (light red and light green) by the conversion RNA/protein ratio  $\approx \Phi_R \cdot 2.1$ . (F) Plot of the ribosome copy number estimated from the proteomic data against the estimated  $\langle \# \text{ori} \rangle$ .

620 Here we attempt to place our observations across the proteomic data sets in the context of *E.*  
621 *coli* maximizing its steady-state growth rate across a wide array of conditions.

622 Parallel DNA replication biases gene dosage in support of ribosome synthesis.  
623 *E. coli* cells grow by a so-called "adder" mechanism, whereby cells add a constant volume with each  
624 cell division (?). In conjunction with this, additional rounds of DNA replication are triggered when  
625 cells reach a critical volume per origin of replication (Figure 10(A)). This leads to the classically-  
626 described exponential increase in cell size with growth rate ????. In the context of maximizing  
627 growth rate, it is notable that the majority of ribosomal proteins and rRNA operons are found  
628 closer to the DNA origin.

629 While an increase in transcription has been observed for genes closer to the origin in rapidly  
630 growing *E. coli* (?), we were unaware of such characterization at the proteomic level. In order to  
631 see whether there is a relative increase in protein expression for genes closer to the origin at  
632 faster growth, we calculated a running boxcar average (500 kbp window) of protein copy number  
633 as a function of each gene's transcriptional start site (Figure 10(B)). While absolute protein copy  
634 numbers can vary substantially across the chromosome, we indeed observe a bias in expression  
635 under fast growth conditions (dark blue), showing the result. The dramatic change in protein copy  
636 number near the origin is primarily due to the increase in ribosomal protein expression. This trend  
637 is in contrast to slower growth conditions (yellow) where the average copy number is more uniform  
638 across the length of the chromosome.

639 If ribosomal genes (rRNA and ribosomal proteins) are being synthesized at their maximal rate  
 640 according to their rRNA gene dosage and maximal transcription rate, we can make two related  
 641 hypotheses about how their ribosome abundance should vary with chromosomal content. First,  
 642 the ribosomal protein fraction should increase in proportion to the average ratio of DNA origins to  
 643 DNA termini ( $\langle \# \text{ ori} \rangle / \langle \# \text{ ter} \rangle$  ratio). This is a consequence of the skew in DNA dosage as cells grow  
 644 faster. The second hypothesis is that the absolute number of ribosomes should increase with the  
 645 number of DNA origins ( $\langle \# \text{ ori} \rangle$ ), since this will reflect the total gene dosage at a particular growth  
 646 condition.

647 In order to test each of these expectations we considered the experimental data from ?, which  
 648 inferred these parameters for cells under nutrient-limited growth. The ratio  $\langle \# \text{ ori} \rangle / \langle \# \text{ ter} \rangle$  de-  
 649 pends on how quickly chromosomes are replicated relative the cell's doubling time  $\tau$  and is given  
 650 by  $2^{\tau_C/\tau}$ . Here  $\tau_C$  is the time taken to replicate *E. coli*'s chromosome, referred to as the C period of  
 651 cell division. In **Figure 10(C)** we plot the measured  $\tau_C$  versus  $\tau$  (computed as  $\tau = \log(2)/\lambda$ ), with data  
 652 points in red corresponding to *E. coli* strain MG1655, and blue to strain NCM3722. ? also measured  
 653 the total RNA to protein ratio which reflects ribosomal abundance and we show that data along  
 654 with other recent measurements from ???. Indeed, we find that the ribosomal fraction increases  
 655 with  $\langle \# \text{ ori} \rangle / \langle \# \text{ ter} \rangle$  (**Figure 10(C)**). We note a systematic difference in the relative abundances  
 656 from ? and ? that was inconsistent with a number of other measurements of total RNA-to-protein  
 657 ratios ( $\approx \Phi_R \times 2.1$  ?) and only show the data from ? and ? for relative ribosome abundances  
 658 (see supplemental section XX for a more complete discussion). For the data shown, the ribosomal  
 659 fraction doesn't increase as much at higher  $\langle \# \text{ ori} \rangle / \langle \# \text{ ter} \rangle$ . Since several rRNA operons are actu-  
 660 ally located approximately half-way between the origin and terminus, the trend may in part be a  
 661 consequence of a diminishing increase in rRNA gene dosage at higher  $\langle \# \text{ ori} \rangle / \langle \# \text{ ter} \rangle$  ratios.

662 We can similarly estimate  $\langle \# \text{ ori} \rangle$ , which depends on how often replication forks are initiated per  
 663 cell cycle. This is given by the number of overlapping cell cycles,  $2^{\tau_{\text{cycle}}/\tau}$ , where  $\tau_{\text{cycle}}$  refers to the total  
 664 time of chromosome replication and cell division. **Figure 10(E)** shows the associated data from ?,  
 665 which we use to estimate  $\langle \# \text{ ori} \rangle$  for each growth condition of the proteomic data. In agreement  
 666 with our expectations, we find that ribosome copy number increases with the estimated  $\langle \# \text{ ori} \rangle$   
 667 (**Figure 10(F)**).

668 While it is difficult to distinguish between causality and correlation, the data is consistent with  
 669 the need for cells to increase their effective rRNA gene dosage in order to grow according to the  
 670 constraint set by Equation 2. These results may also shed some light on the notable increase in  
 671 ribosomal content that is observed when sublethal doses of antibiotics (??). Specifically, if rRNA  
 672 synthesis is rate limiting, and nutrient conditions largely dictate the extent of overlapping DNA  
 673 replication cycles, than addition of antibiotic will lengthen the doubling time and allow an increased  
 674 rRNA synthesis relative to the rate of cell division. In Supplemental Section XX, we consider this  
 675 further using additional data from ?.

676 Regulation of translating ribosomes helps maintain maximal growth according to nutri-  
 677 ent availability.

678 While the above observations show how *E. coli* can vary its ribosomal content to increase growth  
 679 rate, it also presents a challenge in the limit of poorer nutrient conditions. Recall from Equation 3  
 680 that ribosomal content should decrease to zero as growth decreases to zero. While bacteria tend  
 681 to decrease their ribosomal abundance in poorer nutrient conditions, they do so only to some  
 682 fixed, non-zero amount (??). Here we find a minimal ribosomal fraction of  $\approx 0.06$  in the slowest  
 683 growth conditions. From the perspective of a bacterium dealing with uncertain nutrient conditions,  
 684 there is likely a benefit for the cell to maintain some relative fraction of ribosomes to support rapid  
 685 growth as nutrient conditions improve.

686 The challenge however, lies in the cell's ability to maintain growth when ribosomes are in ex-  
 687 cess of the rate that nutrients can be harvested and amino acids synthesized for consumption  
 688 **Figure 11A**. In the limit of poor growth conditions, ribosomes would consume their amino acid

689 supply and be unable to maintain steady-state growth. In reality, *E. coli* is still able to maintain a  
 690 relatively high elongation rate even in stationary phase ( $\approx 8$  AA/s, [\(??\)](#)). A explanation for this is  
 691 that the cell further regulates its biological activity in conditions of stress and nutrient-limitation;  
 692 in particular through the small-molecule alarmones (p)ppGpp [\(?\)](#). In (p)ppGpp null strains, cells  
 693 are unable to grow in nutrient-poor media. Indeed, these small molecules play a role in controlling  
 694 biosynthesis rates throughout the central dogma [NB citations]. Here we explore this further in  
 695 the context of growth by maximizing protein synthesis.

696 We consider slow growth conditions ( $\lambda$  less than  $0.5 \text{ hr}^{-1}$ ) by assuming that the decrease in  
 697 elongation rate is due to a limiting supply of amino acids and a need for the cell to maintain excess  
 698 nutrients for cellular homeostasis under steady-state growth. There is some experimental support  
 699 showing that in poorer nutrient growth conditions, cells have lower amino acids concentrations  
 700 [\(?\)](#). We proceed by coarse graining the cell's amino acid supply as an single, effective rate-limiting  
 701 species (see Supplemental Section XX for a more complete discussion). Under such a scenario, the  
 702 elongation rate can described as simply depending on the maximum elongation rate ( $\approx 17.1$  aa/s,  
 703 [\(??\)](#)), an effective  $K_d$ , and the limiting amino acid concentration  $[AA]_{eff}$ . Specifically, the elongation  
 704 rate is given by,

$$r_t = r_t^{max} \cdot \frac{1}{1 + K_d/[AA]_{eff}}. \quad (4)$$

705 For cells growing in minimal media + glucose, the amino acid concentration is of order 100 mM  
 706 (BNID: 110093, [\(??\)](#)). With a growth rate of about  $0.6 \text{ hr}^{-1}$  and elongation rate of 12.5 aa per second  
 707 [\(?\)](#), we can estimate an effective  $K_d$  of about 40 mM. Ultimately the steady state amino acid concen-  
 708 tration will depend on the difference between the supply of amino acids  $r_{aa}$  and consumption by  
 709 ribosomes  $r_t \cdot R \cdot f_a$ , where  $f_a$  accounts for the possible reduction of actively translating ribosomes.

710 In [Figure 11B](#) we consider how the maximal growth rate and elongation rates vary as a function  
 711 of the number of actively translating ribosomes in this slow growth regime (see Supplemental  
 712 Section XX for a complete description of this model). If we consider  $r_{AA}$  to be reflective of a  
 713 specific growth condition, by considering lines of constant  $r_{AA}$ , we find that cells grow fastest by  
 714 maximizing their fraction of actively translating ribosomes. When we consider the experimental  
 715 measurements from [?](#), we see that although cells indeed reduce  $R \times f_a$ , they do so in a way that  
 716 keeps  $[AA]_{eff}$  relatively constant. Given our estimate for the  $K_d$  of 40 mM, we would only expect  
 717 a decrease from 100 mM to about 35 mM in the slowest growth conditions. While experimental  
 718 data is limited, amino acid concentrations only decrease to about 60 mM for cells grown in minimal  
 719 media + acetate ( $\lambda = 0.3 \text{ hr}^{-1}$  in our proteomic data; value obtained from [?](#)), qualitatively consistent  
 720 with our expectations.

721 Given the quantitative data from [?](#), which determined  $f_a$  across the entire range of growth  
 722 rates across our data, we next estimated the active fraction of ribosomal protein. As shown in [Figure 11\(C\)](#), we find that cells grow at a rate near the expected translation maximum expected from  
 723 Equation 1, using the maximum elongation rate of  $r_t = 17.1$  aa per second. This is in contrast to the  
 724 reality that ribosomes are translating at almost half this rate in the poorest growth conditions. This  
 725 highlights that there are alternative ways to grow according to the translated-limited growth rate  
 726 that is expected based with ribosomes translating at their maximal elongation rate. Specifically, it  
 727 is by adjusting  $r_t \times R \times f_a$  to match maximal growth rate set by Equation 2, through the parameters  
 728  $r_{tmax} \times R'$ , that cells are able to maximize their growth rate under steady-state.

730 Global regulatory control across central dogma may provide an explanation for the robust scaling laws in *E. coli*.

731 A number of recent papers further highlight the possibility that (p)ppGpp may even provide a causal  
 732 explanation for the scaling laws in *E. coli*. In the context of ribosomal activity, increased levels of  
 733 (p)ppGpp are associated with lower ribosomal content, and at slow growth appear to help reduce  
 734 the fraction of actively translating ribosomes [\(??\)](#). Titration of the cellular (p)ppGpp concentrations

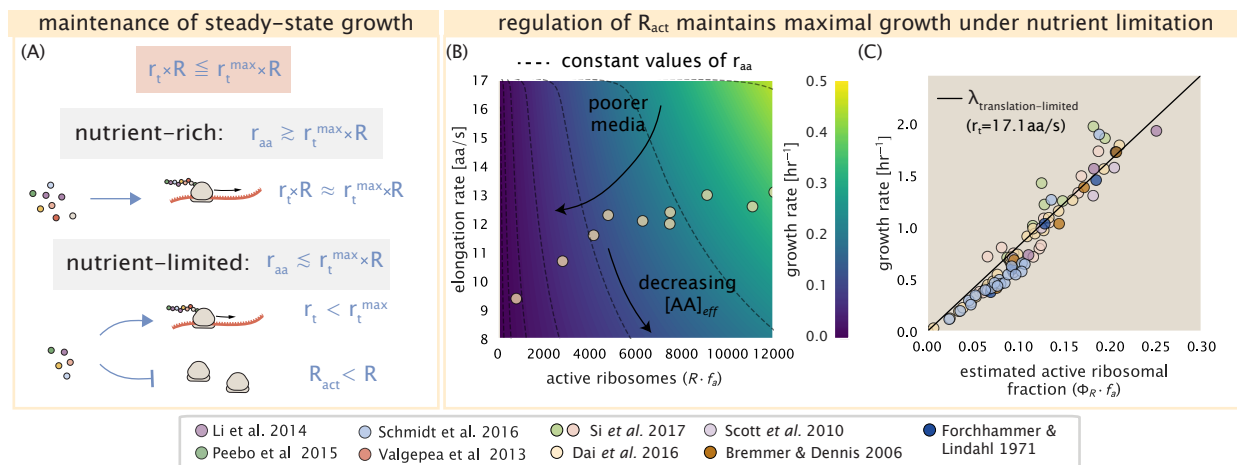


**Figure 11. *E. coli* must regulate ribosomal activity in limiting nutrient conditions.** (A) Schematic showing translation-specific requirements for maintenance of steady-state growth. In a nutrient rich environment, amino acid supply  $r_{aa}$  is sufficiently in excess of the demand by ribosomes translating at their maximal rate. In poorer nutrient conditions, reduced amino acid supply  $r_{aa}$  will decrease the rate of elongation. In a regime where  $r_{aa}$  is less than  $r_t \cdot R$ , the number of actively translating ribosomes will need to be reduced in order to maintain steady-state growth. (B) Translation elongation rate is plotted as a function of the number of actively translating ribosomes  $R \cdot f_a$ . Dashed lines correspond to a range of amino acid synthesis rates  $r_{aa}$ , from  $10^3$  to  $10^6$ . Growth rates are calculated according to Equation 1, assuming a constant ribosomal fraction of 8 percent. See appendix XX for additional details. (C) Experimental data from Dai *et al.* are used to estimate the fraction of actively translating ribosomes. The solid line represents the translation-limited growth rate for ribosomes elongating at 17.1 AA/s.

736 (up or down) can invoke similar proteomic changes reminiscent of those observed under nutrient  
 737 limitation (?). In light of the limiting dependence of ribosome copy number on chromosomal gene  
 738 dosage, it was recently shown that growth in a (p)ppGpp null strain abolishes both the scaling in  
 739 cell size and the  $\langle \# \text{ ori} \rangle / \langle \# \text{ ter} \rangle$  ratio. Instead, cells exhibited a high  $\langle \# \text{ ori} \rangle / \langle \# \text{ ter} \rangle$  closer to 4 and  
 740 cell size more consistent with a fast growth state where (p)ppGpp levels are low (?).]

741 [NB, expand on to consider how activity of RNAP and other aspects(?) may follow a similar  
 742 behaviour and are under related control mechanisms.]

## 743 References

- 744 Abelson, H., Johnson, L., Penman, S., and Green, H. (1974). Changes in RNA in relation to growth of the fibroblast:  
 745 II. The lifetime of mRNA, rRNA, and tRNA in resting and growing cells. *Cell*, 1(4):161–165.
- 746 Aidelberg, G., Towbin, B. D., Rothschild, D., Dekel, E., Bren, A., and Alon, U. (2014). Hierarchy of non-glucose  
 747 sugars in *Escherichia coli*. *BMC Systems Biology*, 8(1):133.
- 748 Antonenko, Y. N., Pohl, P., and Denisov, G. A. (1997). Permeation of ammonia across bilayer lipid membranes  
 749 studied by ammonium ion selective microelectrodes. *Biophysical Journal*, 72(5):2187–2195.
- 750 Ashburner, M., Ball, C. A., Blake, J. A., Botstein, D., Butler, H., Cherry, J. M., Davis, A. P., Dolinski, K., Dwight, S. S.,  
 751 Eppig, J. T., Harris, M. A., Hill, D. P., Issel-Tarver, L., Kasarskis, A., Lewis, S., Matese, J. C., Richardson, J. E.,  
 752 Ringwald, M., Rubin, G. M., and Sherlock, G. (2000). Gene Ontology: tool for the unification of biology. *Nature Genetics*,  
 753 25(1):25–29.
- 754 Ason, B., Bertram, J. G., Hingorani, M. M., Beechem, J. M., O'Donnell, M., Goodman, M. F., and Bloom, L. B.  
 755 (2000). A Model for *Escherichia coli* DNA Polymerase III Holoenzyme Assembly at Primer/Template Ends:  
 756 DNA Triggers A Change In Binding Specificity of the  $\gamma$  Complex Clamp Loader. *Journal of Biological Chemistry*,  
 757 275(4):3006–3015.
- 758 Assentoft, M., Kaptan, S., Schneider, H.-P., Deitmer, J. W., de Groot, B. L., and MacAulay, N. (2016). Aquaporin 4  
 759 as a NH<sub>3</sub> Channel. *Journal of Biological Chemistry*, 291(36):19184–19195.
- 760 Bauer, S. and Ziv, E. (1976). Dense growth of aerobic bacteria in a bench-scale fermentor. *Biotechnology and  
 761 Bioengineering*, 18(1):81–94. \_eprint: <https://onlinelibrary.wiley.com/doi/10.1002/bit.260180107>.
- 762 Belliveau, N. M., Barnes, S. L., Ireland, W. T., Jones, D. L., Sweredoski, M. J., Moradian, A., Hess, S., Kinney, J. B.,  
 763 and Phillips, R. (2018). Systematic approach for dissecting the molecular mechanisms of transcriptional  
 764 regulation in bacteria. *Proceedings of the National Academy of Sciences*, 115(21):E4796–E4805.
- 765 Bennett, B. D., Kimball, E. H., Gao, M., Osterhout, R., Van Dien, S. J., and Rabinowitz, J. D. (2009). Absolute  
 766 metabolite concentrations and implied enzyme active site occupancy in *Escherichia coli*. *Nature Chemical  
 767 Biology*, 5(8):593–599.
- 768 Birnbaum, L. S. and Kaplan, S. (1971). Localization of a Portion of the Ribosomal RNA Genes in *Escherichia coli*.  
 769 *Proceedings of the National Academy of Sciences*, 68(5):925–929.
- 770 Booth, I. R., Mitchell, W. J., and Hamilton, W. A. (1979). Quantitative analysis of proton-linked transport systems.  
 771 The lactose permease of *Escherichia coli*. *Biochemical Journal*, 182(3):687–696.
- 772 Bremer, H. and Dennis, P. P. (2008). Modulation of Chemical Composition and Other Parameters of the Cell at  
 773 Different Exponential Growth Rates. *EcoSal Plus*, 3(1).
- 774 Browning, D. F. and Busby, S. J. W. (2016). Local and global regulation of transcription initiation in bacteria.  
 775 *Nature Reviews Microbiology*, 14(10):638–650.
- 776 Cox, G. B., Newton, N. A., Gibson, F., Snoswell, A. M., and Hamilton, J. A. (1970). The function of ubiquinone in  
 777 *Escherichia coli*. *Biochemical Journal*, 117(3):551–562.
- 778 Dai, X., Zhu, M., Warren, M., Balakrishnan, R., Okano, H., Williamson, J. R., Fredrick, K., and Hwa, T. (2018).  
 779 Slowdown of Translational Elongation in *Escherichia coli* under Hyperosmotic Stress. - PubMed - NCBI. *mBio*,  
 780 9(1):281.
- 781 Dai, X., Zhu, M., Warren, M., Balakrishnan, R., Patsalo, V., Okano, H., Williamson, J. R., Fredrick, K., Wang, Y.-P.,  
 782 and Hwa, T. (2016). Reduction of translating ribosomes enables *Escherichia coli* to maintain elongation rates  
 783 during slow growth. *Nature Microbiology*, 2(2):16231.
- 784 Escalante, A., Salinas Cervantes, A., Gosset, G., and Bolívar, F. (2012). Current knowledge of the *Escherichia coli*  
 785 phosphoenolpyruvate-carbohydrate phosphotransferase system: Peculiarities of regulation and impact on  
 786 growth and product formation. *Applied Microbiology and Biotechnology*, 94(6):1483–1494.
- 787 Feist, A. M., Henry, C. S., Reed, J. L., Krummenacker, M., Joyce, A. R., Karp, P. D., Broadbelt, L. J., Hatzimanikatis,  
 788 V., and Palsson, B. Ø. (2007). A genome-scale metabolic reconstruction for *Escherichia coli* K-12 MG1655 that  
 789 accounts for 1260 ORFs and thermodynamic information. *Molecular Systems Biology*, 3(1):121.

- 790 Fernández-Coll, L., Maciąg-Dorszynska, M., Tailor, K., Vadia, S., Levin, P. A., Szalewska-Palasz, A., Cashel, M.,  
 791 and Dunny, G. M. (2020). The Absence of (p)ppGpp Renders Initiation of *Escherichia coli* Chromosomal DNA  
 792 Synthesis Independent of Growth Rates. *mBio*, 11(2):45.
- 793 Fijalkowska, I. J., Schaaper, R. M., and Jonczyk, P. (2012). DNA replication fidelity in *Escherichia coli*: A multi-DNA  
 794 polymerase affair. *FEMS Microbiology Reviews*, 36(6):1105–1121.
- 795 Finkelstein, I. J. and Greene, E. C. (2013). Molecular Traffic Jams on DNA. *Annual Review of Biophysics*, 42(1):241–  
 796 263.
- 797 Gama-Castro, S., Salgado, H., Santos-Zavaleta, A., Ledezma-Tejeida, D., Muñiz-Rascado, L., García-Sotelo, J. S.,  
 798 Alquicira-Hernández, K., Martínez-Flores, I., Pannier, L., Castro-Mondragón, J. A., Medina-Rivera, A., Solano-  
 799 Lira, H., Bonavides-Martínez, C., Pérez-Rueda, E., Alquicira-Hernández, S., Porrón-Sotelo, L., López-Fuentes,  
 800 A., Hernández-Koutoucheva, A., Moral-Chávez, V. D., Rinaldi, F., and Collado-Vides, J. (2016). RegulonDB  
 801 version 9.0: High-level integration of gene regulation, coexpression, motif clustering and beyond. *Nucleic  
 802 Acids Research*, 44(D1):D133–D143.
- 803 Ge, J., Yu, G., Ator, M. A., and Stubbe, J. (2003). Pre-Steady-State and Steady-State Kinetic Analysis of *E. coli* Class  
 804 I Ribonucleotide Reductase. *Biochemistry*, 42(34):10071–10083.
- 805 Godin, M., Delgado, F. F., Son, S., Grover, W. H., Bryan, A. K., Tzur, A., Jorgensen, P., Payer, K., Grossman, A. D.,  
 806 Kirschner, M. W., and Manalis, S. R. (2010). Using buoyant mass to measure the growth of single cells. *Nature  
 807 Methods*, 7(5):387–390.
- 808 Goldman, S. R., Nair, N. U., Wells, C. D., Nickels, B. E., and Hochschild, A. (2015). The primary  $\sigma$  factor in *Es-  
 809 cherichia coli* can access the transcription elongation complex from solution *in vivo*. *eLife*, 4:e10514.
- 810 Harris, L. K. and Theriot, J. A. (2018). Surface Area to Volume Ratio: A Natural Variable for Bacterial Morphogen-  
 811 esis. *Trends in microbiology*, 26(10):815–832.
- 812 Harris, R. M., Webb, D. C., Howitt, S. M., and Cox, G. B. (2001). Characterization of PitA and PitB from *Escherichia  
 813 coli*. *Journal of Bacteriology*, 183(17):5008–5014.
- 814 Heldal, M., Norland, S., and Tumyr, O. (1985). X-ray microanalytic method for measurement of dry matter and  
 815 elemental content of individual bacteria. *Applied and Environmental Microbiology*, 50(5):1251–1257.
- 816 Henkel, S. G., Beek, A. T., Steinsiek, S., Stagge, S., Bettenbrock, K., de Mattos, M. J. T., Sauter, T., Sawodny, O.,  
 817 and Ederer, M. (2014). Basic Regulatory Principles of *Escherichia coli*'s Electron Transport Chain for Varying  
 818 Oxygen Conditions. *PLoS ONE*, 9(9):e107640.
- 819 Hui, S., Silverman, J. M., Chen, S. S., Erickson, D. W., Basan, M., Wang, J., Hwa, T., and Williamson, J. R. (2015).  
 820 Quantitative proteomic analysis reveals a simple strategy of global resource allocation in bacteria. *Molecular  
 821 Systems Biology*, 11(2):e784–e784.
- 822 Ingledew, W. J. and Poole, R. K. (1984). The respiratory chains of *Escherichia coli*. *Microbiological Reviews*,  
 823 48(3):222–271.
- 824 Ireland, W. T., Beeler, S. M., Flores-Bautista, E., Belliveau, N. M., Sweredoski, M. J., Moradian, A., Kinney, J. B.,  
 825 and Phillips, R. (2020). Deciphering the regulatory genome of *Escherichia coli*, one hundred promoters at a  
 826 time. *bioRxiv*.
- 827 Jacob, F. and Monod, J. (1961). Genetic regulatory mechanisms in the synthesis of proteins. *Journal of Molecular  
 828 Biology*, 3(3):318–356.
- 829 Jensen, R. B., Wang, S. C., and Shapiro, L. (2001). A moving DNA replication factory in *Caulobacter crescentus*.  
 830 *The EMBO journal*, 20(17):4952–4963.
- 831 Jun, S., Si, F., Pugatch, R., and Scott, M. (2018). Fundamental principles in bacterial physiology - history, recent  
 832 progress, and the future with focus on cell size control: A review. *Reports on Progress in Physics*, 81(5):056601.
- 833 Kapanidis, A. N., Margeat, E., Laurence, T. A., Doose, S., Ho, S. O., Mukhopadhyay, J., Kortkhonjia, E., Mekler, V.,  
 834 Ebright, R. H., and Weiss, S. (2005). Retention of Transcription Initiation Factor  $\Sigma$ 70 in Transcription Elonga-  
 835 tion: Single-Molecule Analysis. *Molecular Cell*, 20(3):347–356.
- 836 Khademi, S., O'Connell, J., Remis, J., Robles-Colmenares, Y., Miercke, L.J.W., and Stroud, R. M. (2004). Mechanism  
 837 of Ammonia Transport by Amt/MEP/Rh: Structure of AmtB at 1.35 Å. *Science*, 305(5690):1587–1594.

- 838 Khademian, M. and Imlay, J. A. (2017). *Escherichia coli* cytochrome c peroxidase is a respiratory oxidase that  
839 enables the use of hydrogen peroxide as a terminal electron acceptor. *Proceedings of the National Academy  
840 of Sciences*, 114(33):E6922–E6931.
- 841 Li, G.-W., Burkhardt, D., Gross, C., and Weissman, J. S. (2014). Quantifying absolute protein synthesis rates  
842 reveals principles underlying allocation of cellular resources. *Cell*, 157(3):624–635.
- 843 Liebermeister, W., Noor, E., Flamholz, A., Davidi, D., Bernhardt, J., and Milo, R. (2014). Visual account of protein  
844 investment in cellular functions. *Proceedings of the National Academy of Sciences*, 111(23):8488–8493.
- 845 Liu, M., Durfee, T., Cabrera, J. E., Zhao, K., Jin, D. J., and Blattner, F. R. (2005). Global Transcriptional Programs  
846 Reveal a Carbon Source Foraging Strategy by *Escherichia coli*. *Journal of Biological Chemistry*, 280(16):15921–  
847 15927.
- 848 Maaløe, O. (1979). *Regulation of the Protein-Synthesizing Machinery—Ribosomes, tRNA, Factors, and So On*. Gene  
849 Expression. Springer.
- 850 Milo, R., Jorgensen, P., Moran, U., Weber, G., and Springer, M. (2010). BioNumbers—the database of key num-  
851 bers in molecular and cell biology. *Nucleic Acids Research*, 38(suppl\_1):D750–D753.
- 852 Monod, J. (1947). The phenomenon of enzymatic adaptation and its bearings on problems of genetics and  
853 cellular differentiation. *Growth Symposium*, 9:223–289.
- 854 Mooney, R. A., Darst, S. A., and Landick, R. (2005). Sigma and RNA Polymerase: An On-Again, Off-Again Rela-  
855 tionship? *Molecular Cell*, 20(3):335–345.
- 856 Mooney, R. A. and Landick, R. (2003). Tethering  $\Sigma$ 70 to RNA polymerase reveals high *in vivo* activity of  $\sigma$  factors  
857 and  $\Sigma$ 70-dependent pausing at promoter-distal locations. *Genes & Development*, 17(22):2839–2851.
- 858 Neidhardt, F. C., Ingraham, J., and Schaechter, M. (1991). *Physiology of the Bacterial Cell - A Molecular Approach*,  
859 volume 1. Elsevier.
- 860 Ojkic, N., Serbanescu, D., and Banerjee, S. (2019). Surface-to-volume scaling and aspect ratio preservation in  
861 rod-shaped bacteria. *eLife*, 8:642.
- 862 Patrick, M., Dennis, P. P., Ehrenberg, M., and Bremer, H. (2015). Free RNA polymerase in *Escherichia coli*.  
863 *Biochimie*, 119:80–91.
- 864 Peebo, K., Valgepea, K., Maser, A., Nahku, R., Adamberg, K., and Vilu, R. (2015). Proteome reallocation in *Es-*  
865 *cherichia coli* with increasing specific growth rate. *Molecular BioSystems*, 11(4):1184–1193.
- 866 Perdue, S. A. and Roberts, J. W. (2011).  $\sigma^{70}$ -dependent Transcription Pausing in *Escherichia coli*. *Journal of  
867 Molecular Biology*, 412(5):782–792.
- 868 Phillips, R. (2018). Membranes by the Numbers. In *Physics of Biological Membranes*, pages 73–105. Springer,  
869 Cham, Cham.
- 870 Ramos, S. and Kaback, H. R. (1977). The relation between the electrochemical proton gradient and active trans-  
871 port in *Escherichia coli* membrane vesicles. *Biochemistry*, 16(5):854–859.
- 872 Rosenberg, H., Gerdes, R. G., and Chegwidden, K. (1977). Two systems for the uptake of phosphate in *Escherichia  
873 coli*. *Journal of Bacteriology*, 131(2):505–511.
- 874 Rudd, S. G., Valerie, N. C. K., and Helleday, T. (2016). Pathways controlling dNTP pools to maintain genome  
875 stability. *DNA Repair*, 44:193–204.
- 876 Sánchez-Romero, M. A., Molina, F., and Jiménez-Sánchez, A. (2011). Organization of ribonucleoside diphosphate  
877 reductase during multifork chromosome replication in *Escherichia coli*. *Microbiology*, 157(8):2220–2225.
- 878 Schaechter, M., Maaløe, O., and Kjeldgaard, N. O. (1958). Dependency on Medium and Temperature of Cell Size  
879 and Chemical Composition during Balanced Growth of *Salmonella typhimurium*. *Microbiology*, 19(3):592–606.
- 880 Schmidt, A., Kochanowski, K., Vedelaar, S., Ahrné, E., Volkmer, B., Callipo, L., Knoops, K., Bauer, M., Aebersold,  
881 R., and Heinemann, M. (2016). The quantitative and condition-dependent *Escherichia coli* proteome. *Nature  
882 Biotechnology*, 34(1):104–110.

- 883 Scholz, S. A., Diao, R., Wolfe, M. B., Fivenson, E. M., Lin, X. N., and Freddolino, P. L. (2019). High-Resolution  
884 Mapping of the *Escherichia coli* Chromosome Reveals Positions of High and Low Transcription. *Cell Systems*,  
885 8(3):212–225.e9.
- 886 Scott, M., Gunderson, C. W., Mateescu, E. M., Zhang, Z., and Hwa, T. (2010). Interdependence of cell growth and  
887 gene expression: origins and consequences. *Science*, 330(6007):1099–1102.
- 888 Sekowska, A., Kung, H.-F., and Danchin, A. (2000). Sulfur Metabolism in *Escherichia coli* and Related Bacteria:  
889 Facts and Fiction. *Journal of Molecular Microbiology and Biotechnology*, 2(2):34.
- 890 Si, F., Le Treut, G., Sauls, J. T., Vadia, S., Levin, P. A., and Jun, S. (2019). Mechanistic Origin of Cell-Size Control  
891 and Homeostasis in Bacteria. *Current Biology*, 29(11):1760–1770.e7.
- 892 Si, F., Li, D., Cox, S. E., Sauls, J. T., Azizi, O., Sou, C., Schwartz, A. B., Erickstad, M. J., Jun, Y., Li, X., and Jun, S. (2017).  
893 Invariance of Initiation Mass and Predictability of Cell Size in *Escherichia coli*. *Current Biology*, 27(9):1278–1287.
- 894 Sirko, A., Zatyka, M., Sadowy, E., and Hulanicka, D. (1995). Sulfate and thiosulfate transport in *Escherichia coli* K-  
895 12: Evidence for a functional overlapping of sulfate- and thiosulfate-binding proteins. *Journal of Bacteriology*,  
896 177(14):4134–4136.
- 897 Stasi, R., Neves, H. I., and Spira, B. (2019). Phosphate uptake by the phosphonate transport system PhnCDE.  
898 *BMC Microbiology*, 19.
- 899 Stevenson, B. S. and Schmidt, T. M. (2004). Life History Implications of rRNA Gene Copy Number in *Escherichia*  
900 *coli*. *Applied and Environmental Microbiology*, 70(11):6670–6677.
- 901 Stouthamer, A. H. and Bettenhaussen, C. W. (1977). A continuous culture study of an ATPase-negative mutant  
902 of *Escherichia coli*. *Archives of Microbiology*, 113(3):185–189.
- 903 Svenningsen, S. L., Kongstad, M., Stenum, T. S. n., Muñoz-Gómez, A. J., and Sørensen, M. A. (2017). Transfer RNA  
904 is highly unstable during early amino acid starvation in *Escherichia coli*. *Nucleic Acids Research*, 45(2):793–804.
- 905 Szenk, M., Dill, K. A., and de Graff, A. M. R. (2017). Why Do Fast-Growing Bacteria Enter Overflow Metabolism?  
906 Testing the Membrane Real Estate Hypothesis. *Cell Systems*, 5(2):95–104.
- 907 Taheri-Araghi, S., Bradde, S., Sauls, J. T., Hill, N. S., Levin, P. A., Paulsson, J., Vergassola, M., and Jun, S. (2015).  
908 Cell-size control and homeostasis in bacteria. - PubMed - NCBI. *Current Biology*, 25(3):385–391.
- 909 Tatusov, R. L., Galperin, M. Y., Natale, D. A., and Koonin, E. V. (2000). The COG database: a tool for genome-scale  
910 analysis of protein functions and evolution. *Nucleic Acids Research*, 28(1):33–36.
- 911 Taymaz-Nikerel, H., Borujeni, A. E., Verheijen, P. J. T., Heijnen, J. J., and van Gulik, W. M. (2010).  
912 Genome-derived minimal metabolic models for *Escherichia coli* mg1655 with estimated in vivo  
913 respiratory ATP stoichiometry. *Biotechnology and Bioengineering*, 107(2):369–381. \_eprint:  
914 <https://onlinelibrary.wiley.com/doi/pdf/10.1002/bit.22802>.
- 915 The Gene Ontology Consortium (2018). The Gene Ontology Resource: 20 years and still GOing strong. *Nucleic  
916 Acids Research*, 47(D1):D330–D338.
- 917 Valgepea, K., Adamberg, K., Seiman, A., and Vilu, R. (2013). *Escherichia coli* achieves faster growth by increasing  
918 catalytic and translation rates of proteins. *Molecular BioSystems*, 9(9):2344.
- 919 van Heeswijk, W. C., Westerhoff, H. V., and Boogerd, F. C. (2013). Nitrogen Assimilation in *Escherichia coli*: Putting  
920 Molecular Data into a Systems Perspective. *Microbiology and Molecular Biology Reviews*, 77(4):628–695.
- 921 Weber, J. and Senior, A. E. (2003). ATP synthesis driven by proton transport in F1FO-ATP synthase. *FEBS Letters*,  
922 545(1):61–70.
- 923 Willsky, G. R., Bennett, R. L., and Malamy, M. H. (1973). Inorganic Phosphate Transport in *Escherichia coli*: Involvement  
924 of Two Genes Which Play a Role in Alkaline Phosphatase Regulation. *Journal of Bacteriology*, 113(2):529–  
925 539.
- 926 Zhang, L., Jiang, W., Nan, J., Almqvist, J., and Huang, Y. (2014a). The *Escherichia coli* CysZ is a pH dependent sulfate  
927 transporter that can be inhibited by sulfite. *Biochimica et Biophysica Acta (BBA) - Biomembranes*, 1838(7):1809–  
928 1816.
- 929 Zhang, Z., Aboulwafa, M., and Saier, M. H. (2014b). Regulation of crp gene expression by the catabolite repres-  
930 sor/activator, cra, in *Escherichia coli*. *Journal of Molecular Microbiology and Biotechnology*, 24(3):135–141.
- 931 Zhu, M. and Dai, X. (2019). Growth suppression by altered (p)ppGpp levels results from non-optimal resource  
932 allocation in *Escherichia coli*. *Nucleic Acids Research*, 47(9):4684–4693.